A 15.3 GHz SATELLITE-TO-GROUND DIVERSITY PROPAGATION EXPERIMENT USING A TERMINAL SEPARATION OF 4 KILOMETERS

K.R. Grimm and D.B. Hodge

The Ohio State University

ElectroScience Laboratory

Department of Electrical Engineering
Columbus, Ohio 43212

TECHNICAL REPORT 2374-7

December 1971

Grant Number NGR 36-008-080

National Aeronautics and Space Administration
Office of Grants and Research Contracts
Washington, D.C. 20546

REPORT

by

The Ohio State University ElectroScience Laboratory-188
(Formerly Antenna Laboratory) - 113
Columbus, Ohio 43212 - 65

Sponsor	National Aeronautics and Space Administration Office of Grants and Research Contracts Washington, C.C. 20546
Grant Number	NGR 36-008-080
Investigation of	Millimeter-Wavelengths Propagation Studies
Subject of Report	A 15.3 GHz SATELLITE-TO-GROUND DIVERSITY PROPAGATION EXPERIMENT USING A TERMINAL SEPARATION OF 4 KILOMETERS
Authors	K.R. Grimm and D.B. Hodge
Submitted by	K.R. Grimm and D.B. Hodge ElectroScience Laboratory Department of Electrical Engineering The Ohio State University
Date	December 1971

ABSTRACT

The transmission of microwave energy through the earth's atmosphere is subject to attentuation by the various atmospheric gases and liquid water. At 15.3 GHz severe attenuation due to precipitation is often encountered; therefore, two or more terminals may be used in a switched-path diversity scheme in order to circumvent regions of locally intense rainfall. This diversity technique is currently under investigation at the Ohio State University Electro-Science Laboratory in conjunction with the NASA Goddard Space Flight Center Applications Technology Satellite (ATS-5) Millimeter Wave Experiment. The objective of the Ohio State University participation in the NASA study is to collect 15.3 GHz downlink propagation data and to generate diversity link performance statistics. The purpose of this report is to present the analysis of data collected at Columbus, Ohio, during June and July, 1970. These results characterize the performance of a path diversity satellite-to-ground millimeter wave link with two ground terminals separated by 4 km. At this separation distance the duration of fades below 6 dB was decreased by at least a factor of 10 when using path diversity and the cumulative cross-correlation between the attenuations observed at the two terminals during rain events was approximately 0.45. Narrow beam radiometers directed along the propagation paths were also utilized to relate the path radiometric temperature to the path attenuation.

TABLE OF CONTENTS

CHAPTER I
INTRODUCTION

The successful utilization of the millimeter wave portion of the spectrum for satellite communication systems is dependent upon the specification of fade margins which will result in reliable performance when the link is subjected to precipitation attenuation. It has been experimentally shown that fade depths, depending on the operating frequency and rain rate along the path, may be quite large; for example, the attenuation rate may be on the order of 6 dB/km at 15.3 GHz for a rain rate of 100 mm/hr.[1]

In the region 10 to 100 GHz the complex dielectric constant of liquid water is quite frequency dependent, and, as frequency increases through that range, liquid water becomes quite lossy. As a consequence both absorption and scattering may be significant attenuating mechanisms depending on the signal wavelength and the liquid water drop sizes. In addition to the precipitation attenuation, a millimeter wave will also suffer attenuation due to absorption by the various constituent atmospheric gases. In this frequency range the water vapor and oxygen resonance lines predominate with peak absorption occurring at 22 GHz for water vapor and 60 GHz for molecular oxygen.

For wavelengths much larger than drop sizes, precipitation scattering may be neglected. However, the magnitude of precipitation attenuation by absorption is approximately proportional to the number of drops in the path and can be significantly larger than attenuation due to atmospheric gases. A comparison of the relative contributions to atmospheric attenuation due to gas resonance absorption and due to precipitation has been presented by Mondre as shown in Fig. 1.[2] In this figure curves for attenuation as a function of frequency and rain rate were predicted theoretically from a model investigated by Weibel and Dressel.[3] The curves for attenuation by atmospheric water vapor and molecular oxygen absorption were calculated from the Van Vleck equation.[4,5] These curves demonstrate that the atmospheric gas attenuation rate at 15.3 GHz, for example, may be quite small when compared with the attenuation rate resulting from precipitation.

The successful utilization of millimeter wave lengths on satellite-to-ground paths depends primarily upon the development of effective methods for maintaining sufficiently reliable operations during periods of intense rainfall at the ground terminals. Component size and weight restrictions imposed on the design of a communications satellite will limit that repeater's ability to provide sufficient margin to overcome the precipitation attenuation. Furthermore, improving the ground terminal performance in order to provide sufficient margin may require excessive sophistication or expense.

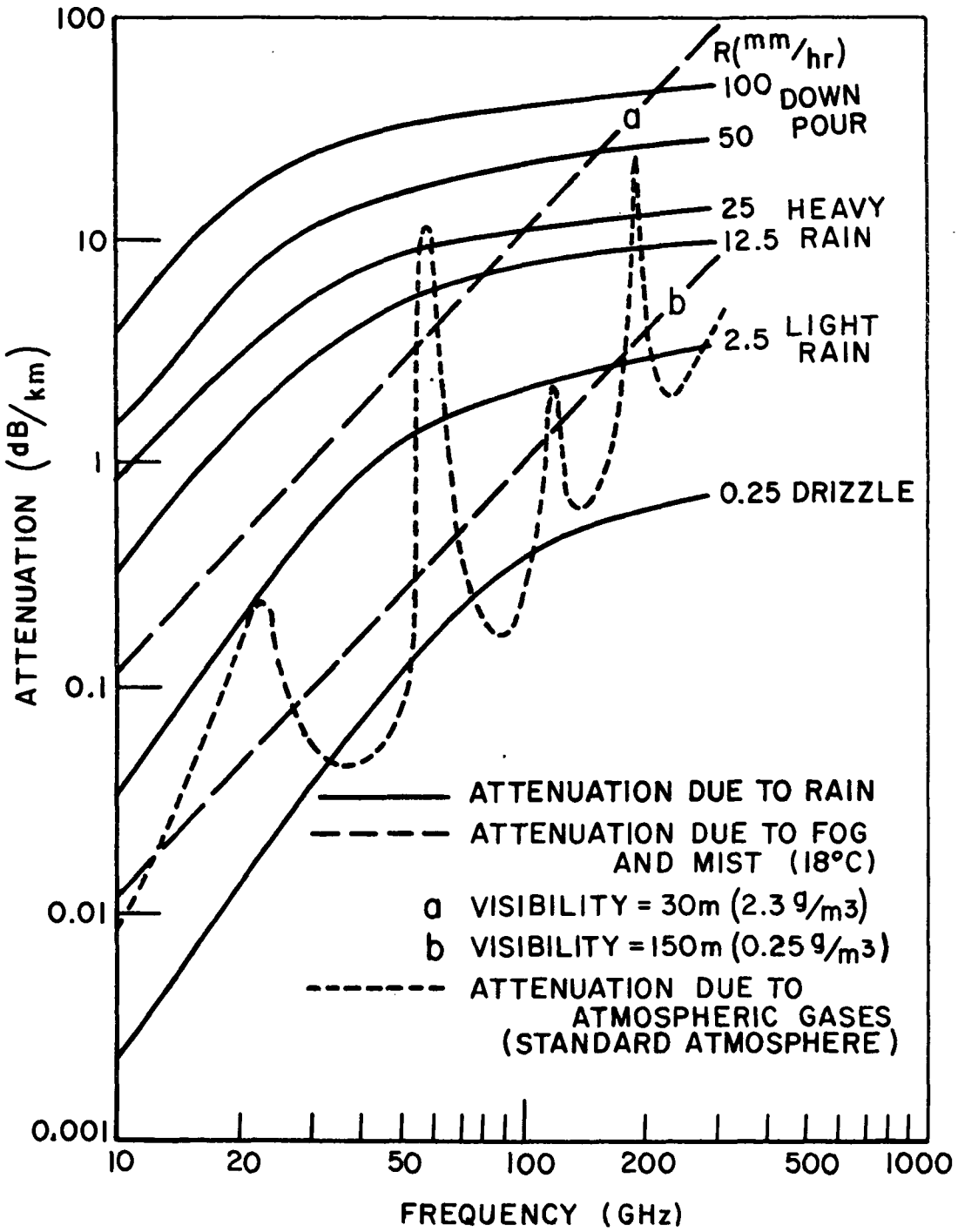

Fig.1--Attenuation due to gas absorption, fog and mist, and rain at millimeter wave frequencies (from Mondre,[2]).

Consequently, the path diversity scheme using two or more terminals sufficiently separated to provide an acceptably low attenuation level on at least one of the paths is a useful alternative for reducing the effect of precipitation attenuation.

The diversity advantage in terrestrial applications can be predicted by measuring the rain rate along the separate paths and then computing and comparing the resulting attenuations.[6] In these applications the accuracy of the estimate of attenuation is dependent upon knowing the rain rate along the path with adequate resolution. However, for satellite-to-ground paths the distribution in time and space of the rain rate along the elevated path through the atmosphere is not known. Consequently a theoretical analysis of a space diversity satellite link operating at millimeter wavelengths is of marginal value until more detailed knowledge of spatial and temporal rain rate distributions is available.

Among the objectives of the NASA ATS-5 Millimeter Wave Experiment is the measurement of precipitation attenuation at various locations in the nation. From these measurements a model may be developed as a prediction tool for satellite communication system designers wishing to utilize this portion of the spectrum. An additional objective of the Ohio State University experiment is the determination of the extent of the reliability improvement provided by path diversity for such a system. Two complete receive-only ground terminals, one fixed and one transportable, have been instrumented for this purpose.[7,8,9] The transportable terminal is completely

self-contained and may be operated at any site where power is available; consequently, both the site separation distance and direction may be varied. Data collected during 7 rain periods in June and July, 1970, using a 4 km site separation have been analyzed and are discussed in this report. A preliminary analysis of portions of these data is also available in Reference [10].

Single terminal performance is analyzed by computing the measured attenuation and fade duration distributions. Diversity performance is analyzed by computing the joint attenuation distribution (instantaneously selecting the signal suffering the least attenuation), the distribution of attenuation at one site with the condition that the second site is at a specified signal level, and the cross-correlation of the attenuation events. The usefulness of the coincident volume Ku-band radiometers installed at the Ohio State University terminals as tools for predicting precipitation attenuation has also been investigated. And, finally, computations of the mean absorption temperature along the propagation path, based on measured attenuation and radiometric temperature, have been performed.

CHAPTER II
THEORETICAL BACKGROUND

A. Attenuation in the Atmosphere

The attenuation of a millimeter wave propagating through the earth's atmosphere is due to:

i. precipitation absorption and scattering

ii. atmospheric gas absorption

iii. atmospheric inhomogeneities.

Rain is the most conspicuous absorber of millimeter wave energy, although the effects of hail, snow, and melting snow may not be entirely ignored.[11] Millimeter wave attenuation by rain depends upon the scattering and absorption cross sections of the individual rain drops. A simple model considering the rain drops to be spherical in shape, situated in a homogeneous medium, and having a complex index of refraction was adapted by Ryde and Ryde from an analysis first given by Mie. This approach, incorporating the drop size distribution and terminal velocities of the drops, has been well summarized by Medhurst,[12] who notes that the theory tends to consistently underestimate the measured attenuation. Further efforts to refine and improve this model have been described by Straiton, Scarpero, and Vogel.[14] In practice the most severe problem encountered in the prediction of millimeter wave precipitation

attenuation is due to the lack of detailed knowledge of the spatial and temporal distribution of the rain rate. Consequently, techniques for predicting precipitation attenuation for system applications will ultimately depend upon the development of methods for relating these characteristics to the rather coarse weather bureau rain rate data which are widely available.

As already pointed out, only water vapor and oxygen are effective absorbers having spectral lines in the region 10 to 100 GHz. However, these lines are not discrete but are spread over a range of frequencies; and, thus, line shape and width factors modify exact calculations for attenuation due to molecular gas absorption. Van Vleck has given expressions for the line width factors which include experimentally determined parameters dependent upon pressure and temperature.[4,5] Other gases, e.g., SO_2, O_3 N_2O, and NO_2, have absorption line spectra in the millimeter wave region, but their relative densities in the atmosphere make attenuation due to these constituents negligible. From Fig. 1, the dashed curve shows that a millimeter wave having a frequency in one of the propagation pass-bands (minima of the gas absorption curve) will not experience attenuation rates greater than approximately 0.2 dB/km due solely to atmospheric gas absorption for frequencies up to 100 GHz. In addition, for satellite paths the total attenuation also falls off rapidly with elevation angle due to the decreasing density of the gases as height increases.

Received signal degradation resulting from random amplitude or phase fluctuations may also occur on millimeter wave paths. These variations are caused by multipath effects and changes in the refractive index due to water vapor along the path.[14] However the reduction in absolute signal level from all effects of medium inhomogeneities is small on elevated paths and is essentially negligible for path elevations exceeding approximately 30°.

B. Attenuation and Path Radiometric Temperature

The feasibility of employing radiometric temperature measurements to predict attenuation on millimeter wave paths has been widely investigated, e.g, Wilson[17] and Altschuler, Wulfsberg, and Falcone.[18] In most cases, the motivation for these investigations has been the instrumentation convenience inherent with the use of small aperture, passively operating radiometers. However, measurements obtained with apertures of a conveniently small size may be only partially effective for predicting millimeter wave attenuation. Such wide beam instruments tend to integrate the radiometric temperature over a spatial region much larger than that directly influencing the line-of-sight signal.

The Ohio State University's large aperture, 15.3 GHz radiometers were designed to permit temperature measurements more closely representative of the true brightness temperature along the propagation path (see Chapter III). The functional relationship between radiometric path temperature and wave attenuation is briefly reviewed in the next paragraphs.

Neglecting scattering effects, the differential equation for the received radiation intensity, I, in terms of the atmospheric absorption coefficient, α, and the brightness of the atmosphere, B, at frequency, f, is:[11]

$$(1) \qquad \frac{dI}{d\ell} = -\alpha[I - B(T)]$$

where the brightness, B(T), is the radiation intensity of a black body at temperature, T, and ℓ is distance along the propagation path. Solving Eq. (1), the received radiating intensity becomes

$$(2) \qquad I = \int_0^\infty B(\ell)\, \alpha(\ell)\, e^{-\int_0^\ell \alpha(\ell')d\ell'}\, d\ell$$

if noise sources other than the atmosphere, e.g., the sun, moon, etc., are ignored and it is assumed that the atmosphere extends to infinity. In this solution the absorption coefficient, $\alpha(\ell)$, and the physical temperature dependence of the brightness, $B(\ell)$, have been expressed as explicit functions of position, ℓ, along the path.

As a consequence of the Rayleigh-Jeans approximation, the Planck's function for black body emission brightness, B, reduces to

$$(4) \qquad B = \frac{2hf^3}{c^2\left(e^{\frac{hf}{kT}} - 1\right)} \approx \frac{2hf^3}{c^2 \frac{hf}{kT}} = 2kT\, \frac{f^2}{c^2}$$

where h = Planck's constant = 6.63×10^{-34} watt-sec^2

c = velocity of light = 2.998×10^{8} m/sec

k = Boltzmann's constant = 1.38×10^{-23} wat-sec^2/°K

T = absolute temperature in degrees Kelvin.

The expression in Eq. (4) is valid for $\frac{hf}{kT} << 1$, which requires $T >> \frac{fx10^{-9}}{8}$. For the 15.3 GHz downlink from ATS-5, this results in required values of $T >> 1.91$°K. Since the path radiometric temperatures under the conditions of this experiment are always significantly above this value, Eq. (4) may be readily applied. As a consequence of Eq. (4), the brightness temperature, T_B, may be defined in the following manner,

$$I = 2k\frac{f^2}{c^2} T_B \quad . \tag{5}$$

Substituting Eqs. (4) and (5) into Eq. (2), an expression for the brightness temperature in terms of the atmospheric temperature results,

$$T_B = \int_0^\infty T(\ell)\, \alpha(\ell)\, e^{-\int_0^\ell \alpha(\ell')d\ell'}\, d\ell \quad . \tag{6}$$

The brightness temperature given by Eq. (6) represents radiation received from within an infinitesimal solid angle of the atmosphere. For practical antennas, however, radiation is received from all directions. Therefore, the brightness temperature, T_B, must be weighted by the antenna gain pattern function to yield the effective brightness temperature,

$$(7) \qquad T_{B_{eff}}(\theta,\phi) = \frac{\int T_B(\theta',\phi')G(\theta,\phi;\theta',\phi')d\theta'd\phi'}{\int G(\theta,\phi;\theta',\phi')d\theta'd\phi'}$$

where T_B is given by Eq. (6), $G(\theta,\phi;\theta',\phi')$ is the antenna gain in the direction (θ',ϕ') with respect to the antenna axis, (θ,ϕ), and the integration extends over all solid angles.

The quantity $T_{B_{eff}}$ is measured by the radiometers used with the Ohio State University ATS-5 terminals. The primary contribution to the measured radiometric temperature is due to the rain in the volume of the antenna pattern; however, $T_{B_{eff}}$ also includes contributions due to atmospheric gases and the ground. The magnitude of these clear weather contributions also depends on the frequency and the antenna elevation angle.

Wulfsberg has averaged many measurements of the clear weather brightness temperature as a function of zenith angle for various frequencies (see Fig. 2).[20] Listed on Fig. 2 are surface temperature, T_g, and relative humidity, ρ. For an elevation angle of approximately 40° to the ATS-5 satellite from Columbus, Ohio, the clear weather sky temperature does not exceed 11°K. This corresponds to an attenuation of 0.16 dB and is negligibly small compared to the magnitude of precipitation attenuation predicted for even moderate rain rates.

Equation (6) may be simplified if the assumption is made that a homogeneous absorbing medium exists along a path of length ℓ. As a consequence of this assumption α and T become independent of path

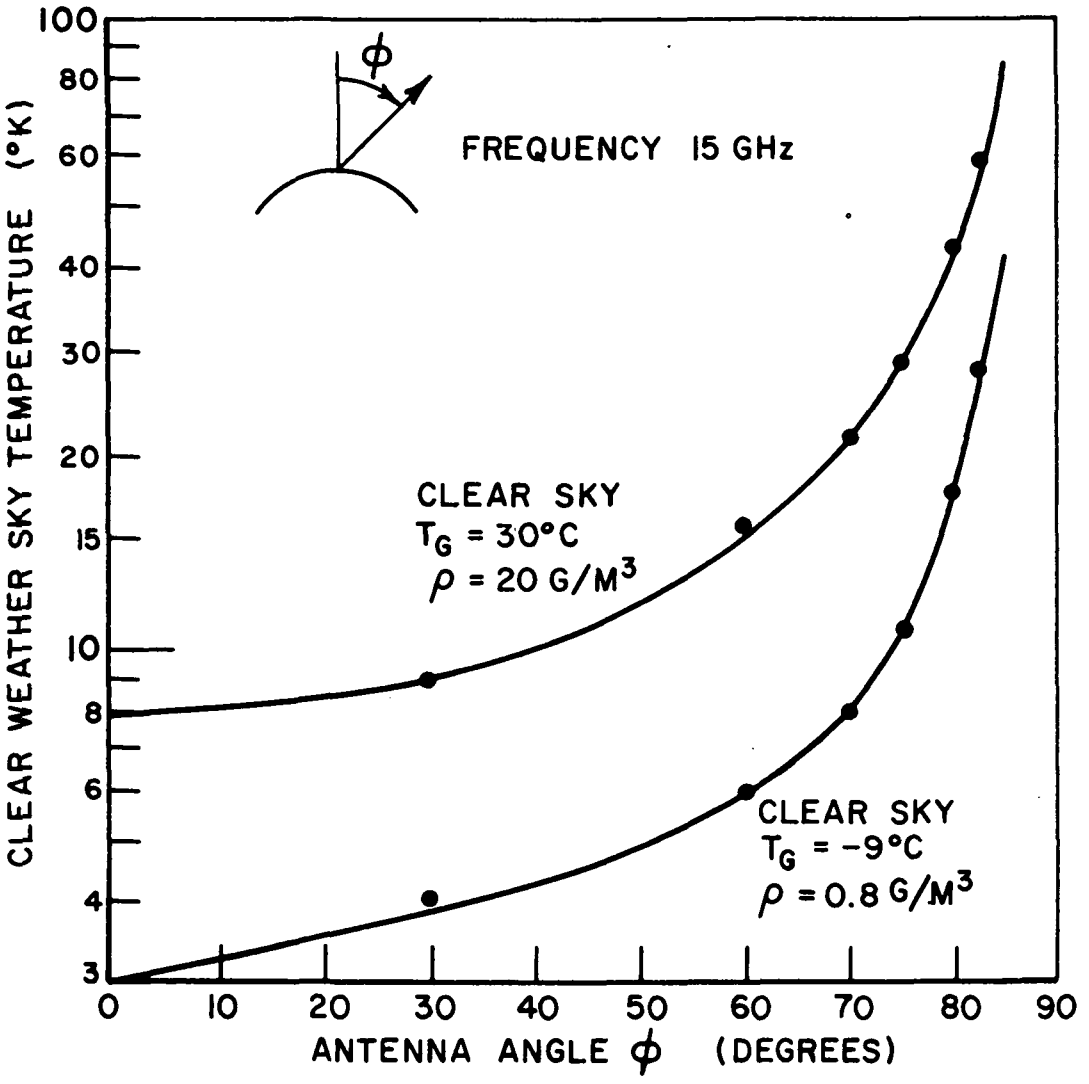

Fig. 2.--Sky temperature profiles at 15 GHz (from Wulfsberg,[20]).

position. In this case T is referred to as the mean absorption temperature, T_m. Equation (6) now becomes

$$T_B = T_m(1 - e^{-\alpha \ell}). \tag{8}$$

Total attenuation along the path is given by the product $A = \alpha\ell$ and, expressed in decibels, is

$$(9) \qquad A = 10 \log_{10}\left(\frac{T_m}{T_m - T_B}\right) \text{ [dB]}.$$

The range of validity for Eq. (9) is not yet fully resolved. Wilson reports a measured upper limit of about 12 dB using data acquired from sun tracker experiments.[21] Ippolito reports good agreement between measured and predicted attenuation values up to 15 dB for most storms.[22] Above this value the attenuation becomes a very sensitive function of both T_m and T_B. Furthermore, for more intense rains, the assumption of homogeneity along the propagation path becomes less realistic.

If Eq. (8) is solved for the mean absorption temperature and T_B is approximated by $T_{B_{eff}}$, an empirical method exists for computing values of T_m. Thus

$$(10) \qquad T_m = \frac{T_{B_{eff}}}{1 - 10^{-A/10}}$$

Where A is the measured attenuation (dB) and $T_{B_{eff}}$ is the simultaneously measured path radiometric temperature. The replacement of T_B by $T_{B_{eff}}$ implies that temperature contributions due to antenna loss and side and back lobes are negligible. This assumption introduces a degree of uncertainty into the direct usage of measured radiometric temperatures although this uncertainty decreases as T_B increases along the propagation path. Results of empirical computations of T_m

as a function of measured attenuation and path temperature are given in Chapter V.

Another useful method for estimating T_m in a clear atmosphere has been given by Wulfsberg.[20] In this approach, the mean absorption temperature for the clear atmosphere is computed from the relation

$$T_m = \frac{\int_0^A T\, e^{-\tau}\, d\tau}{1 - e^{-A}} \tag{11}$$

where T is the temperature at a given point on the path, τ is the absorption integrated over the path to the same point, and A is the absorption evaluated at the surface. Wulfsberg used values of T as a function of height from the standard atmosphere model. The absorption, τ, was computed by evaluating the coefficients of molecular resonance absorption due to water vapor and oxygen concentrations in the standard atmosphere. Thus τ depends on atmospheric profiles of humidity, oxygen, and temperature. Wulfsberg's evaluation of Eq. (11) for various surface temperatures and humidities at 15, 17, and 35 GHz showed that T_m could be reasonably described by a simple expression linear in the ground temperature, T_g,

$$T_m = 1.12\, T_g - 50\ (^\circ K). \tag{12}$$

Equation (12) was developed by Wulfsberg for use in predicting brightness temperature under conditions of no precipitation. However,

propagation measurements made in this study have shown that Eq. (12) appears to be useful even when rain does exist on the path. These results are discussed in Chapter V.

CHAPTER III
EXPERIMENTAL CONFIGURATION

The preparations for the Ohio State University participation in the NASA Goddard Space Flight Center ATS-5 Millimeter Wave Propagation Experiment and progress of the instrumentation phase are documented in References [8] and [9]. Comprehensive descriptions of both the NASA experiment test plan and specifications for the hardware employed in the ground and space terminals may be found in Reference [23]. The test procedures and data collection methods are presented in Reference [24]. A brief summary of the Ohio State University fixed and transportable terminals as they were instrumented during the 1970 data period follows.

The fixed terminal utilized a 30 ft parabolic antenna, manually steerable in azimuth and elevation. The 3 dB beamwidth of this antenna, as measured using the satellite signal, was approximately 0.15° in both azimuth and elevation planes. The phase lock loop receiver was supplied by NASA and was modified slightly to permit manual control of the VCXO during acquisition. The terminal was also equipped with a 15.3 GHz Dicke radiometer designed and built at Ohio State University. This unit was structurally integrated in the RF feed package in order to simultaneously operate with the same receiving aperture as the 15.3 GHz PLL receiver, one polarization

being fed to the receiver and the orthogonal polarization being fed to the radiometer. A square corrugated feed horn was designed and installed as a means of achieving nearly identical E- and H-plane patterns while at the same time insuring low sidelobe level.

Data channel commutators and a 14 track magnetic tape recorder provided a permanent analog record of all propagation and station-keeping data collected during data runs. Following the data runs selected analog data channels were played back for conversion to digital format (see Chapter IV). At the time of digitization the initial processing, including peak detection of the received signal pulses, was accomplished using a small H-P computer. This digital data was then stored on magnetic tape for subsequent processing on an IBM 360-75 machine. At the time of data acquisition several of the analog data channels were also recorded on paper strip charts for the use of the operator and as a backup in case the magnetic tape data was inadvertently lost.

A manually steerable (90° PPI) K_u-band weather radar was available at the fixed site for use as a surveillance instrument. The capability of recording integrated radar backscatter data was not implemented during the 1970 test runs.

The transportable terminal was nearly identical to the fixed terminal with the exception that a 15 ft parabolic antenna provided measured 3 dB beamwidths of approximately 0.3° in both the elevation and azimuth planes. This terminal also contained meterological instrumentation for measuring rain rate, temperature, humidity, wind speed, and wind direction but did not include a weather radar.

The link parameters for the ATS-5 downlink are documented in Reference [22]. Uncertainties associated with several of these parameters for the Ohio State University terminals preclude accurate theoretical predictions of expected absolute received signal levels. These uncertainties include: (1) absolute ground terminal antenna gain, (2) received signal loss due to ground terminal antenna pointing error, (3) PLL receiver response to the pulsed signal, (4) spacecraft transmitter power variations, and a diurnal signal variation of almost 4 dB resulting from a slight inclination of the satellite spin axis.

The top view and side view of the site locations for the Ohio State University terminals are shown in Figs. 3 and 4. During the 1970 data runs, the transportable terminal was located at Site #1. The orientation of the propagation paths was oblique with respect to the direction of site separation; and the direction of separation of the terminals was along an azimuth of 318° from the fixed site.

The goal sought in choosing the Site #1 location was to realize a correlation between fades at the two terminals of approximately 0.50. Although this is not a desirable criterion for the establishment of an operational diversity system this approach would yield more information about the dependence of the correlation upon the site separation distance than the use of extremely small or large separations. This decision was also based on the fact that no diversity data for elevated paths existed prior to these measurements. The selection of the particular site separation distance was based upon

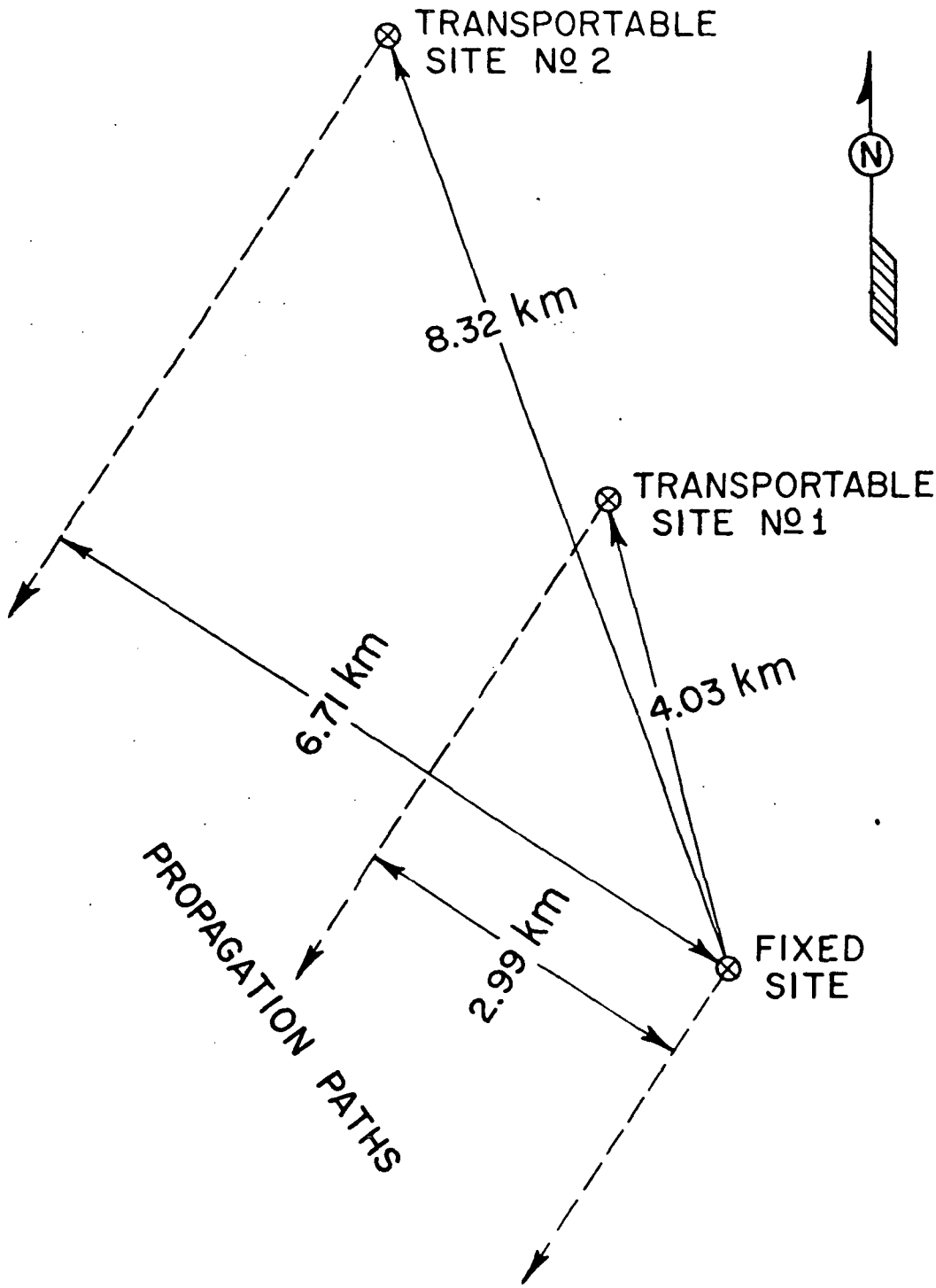

Fig. 3.--Top view of site locations.

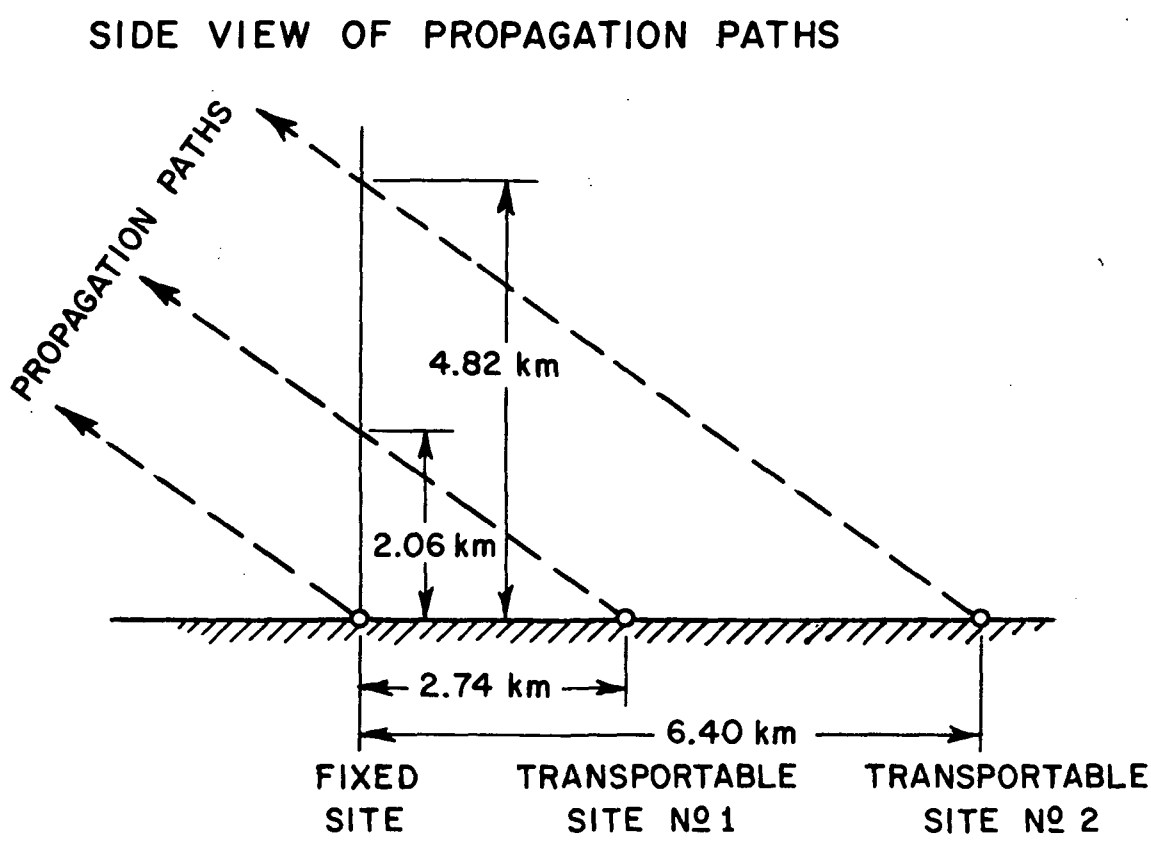

SITE	PATH SEPARATION		
	HORIZONTAL	VERTICAL	SPATIAL
Nº 1	2.99 km	2.06 km	3.41 km
Nº 2	6.71 km	4.82 km	7.73 km

Fig. 4.--Side view of propagation paths.

empirical data describing the spatial behavior of rain rates.[25] The separation distance was 4.03 km.

Typical pointing angles to the synchronous ATS-5 satellite from Columbus, Ohio, are 40° in elevation and 212° in azimuth. The small orbital motion of the spacecraft required that the narrow beam ground terminal antennas be manually repositioned approximately every 10 minutes. Each terminal required a single operator and both terminals were operated during approximately 60 per cent of the time during which precipitation occurred in June and July, 1970. During this time carrier data was recorded with the spacecraft's main transmitter operating.

CHAPTER IV
EXPERIMENT AND ANALYSIS TECHNIQUES

A. Data Collection

Millimeter wave propagation measurements of the received signal from the NASA ATS-5 satellite were first made at the Ohio State University on November 25, 1969, using the transportable terminal. Single terminal operation using the transportable terminal continued through May 16, 1970. During this period 18 test runs were conducted, and a total of 98 hours, 46 minutes of carrier data was recorded. Data from these test runs show little signal fluctuation due to precipitation attenuation since they were collected during the dry winter months.

Two-site operation began at Ohio State University on May 25, 1970. Test runs were conducted simultaneously at both sites and data was recorded on magnetic tape and paper strip charts during the days listed in Table 1. The time entries indicate periods of simultaneous operation during a given test run. A total of 80 hours, 25 minutes of two-site data was recorded during 12 test runs extending over a period from May 25 to October 14, 1970. All of the data except the 25 hours from test run 8 were digitized for further processing. Test run 8 was conducted as a special study of the diurnal variation of the spacecraft signal and is excluded from consideration in this

TABLE 1
TWO-SITE 1970 DATA SUMMARY FOR OSU ATS-5 MILLIMETER WAVE TERMINALS

Test Run	Calendar Day (1970)	GMT (hours)	Tape Number		Remarks
			Transportable	Fixed	
1	June 11, 1970 d 162	1655-2400Z	20	01(B*)	-
2	June 12, 1970 d 163	2235-2350	21	02(C)	-
3	June 14, 1970 d 165	1915-2400	22	03(D)	-
4	June 15, 1970 d 166	0152-1240	23	04(E)	Diversity Fade Periods #1 (0611 to 0641Z) #2 (0941 to 1025Z)
5	June 15, 1970 d 166/167	2121-0206	24	05(F)	-
6	June 17, 1970 d 168/169	2223-0510	25	06(G)	Diversity Fade Periods #3 (2224 to 2334Z) #4 (0128 to 0201Z)
7	June 25, 1970 d 176	1341-1745	26	07(H)	-
8	July 6/7, 1970 d 187/188	d 187 2253- d 188 2400	28 29 30	08(I) 09(J) 10(K)	Special Spacecraft Test Diurnal Signal Variation
9	July 8, 1970 d 189/190	1713-0148	31	11(L)	Diversity Fade Periods #5 (11151 to 11803Z) #6 (1924 to 2000Z)
10	July 18, 1970 d 196/197	2219-0045	32	12(M)	Diversity Fade Period #7 (2224 to 2302Z)
11	July 20, 1970 d 201	1337-1847	33	13(N)	-
12	October 14, 1970 d 287	1355-1450	35	14(O)	-

*OSU Fixed Site Tape Designator

report. An additional period of 1 hour, 45 minutes of two-site data in the 12 test runs is not useful for diversity analysis because high wind speeds necessitated the raising of the fixed site antenna. Forty-eight minutes of two-site data were also lost during periods when the spacecraft transmitter was not operating. Thus, from the 12 two-site test runs conducted in the period May to October, 1970, approximately 63 hours of propagation data were available for two-site analysis. Of this total 270 minutes (4.5 hours) of clearly discernible carrier attenuation occurred at either or both sites. This particular portion of the data has been selected for the diversity study.

An example of the real time strip chart recording of the propagation data is shown in Fig. 5. The upper trace for each site is the voltage output of the 15 GHz radiometer with the ordinate labeled in degrees Kelvin. The lower trace in each case is the pulse-by-pulse receiver carrier level with the 0 dB level corresponding to approximately -120 dBm at the fixed site and -124.5 dBm at the transportable site. The data recorded between the times 2224 to 2334 GMT has been identified as diversity fade period #3. From approximately 2350-0010Z the ATS-5 satellite transmitter was turned off. During the period 0115-0130Z and again just after 0200Z the fixed site antenna was raised due to high wind speeds. Six additional diversity fade periods have been identified from data recorded during test runs 4, 9, and 10. Computer-produced plots of these data after digitization and peak-detection are shown in Fig. 6. The curves in these figures have been averaged over a period of ten satellite pulses, i.e., 7.8 seconds. The time of the beginning of each fade period is noted just below the origin of the relative time scale on the abscissa. The crosshatch marks indicate periods when the 15.3 GHz PLL receiver momentarily lost lock or when the attenuated signal level dropped below the receiver threshold. The curves in Figs. 5 and 6 summarize the two-site fade periods recorded in June and July, 1970. These fade periods are the basis for the diversity analysis with terminals separated by 4 km.

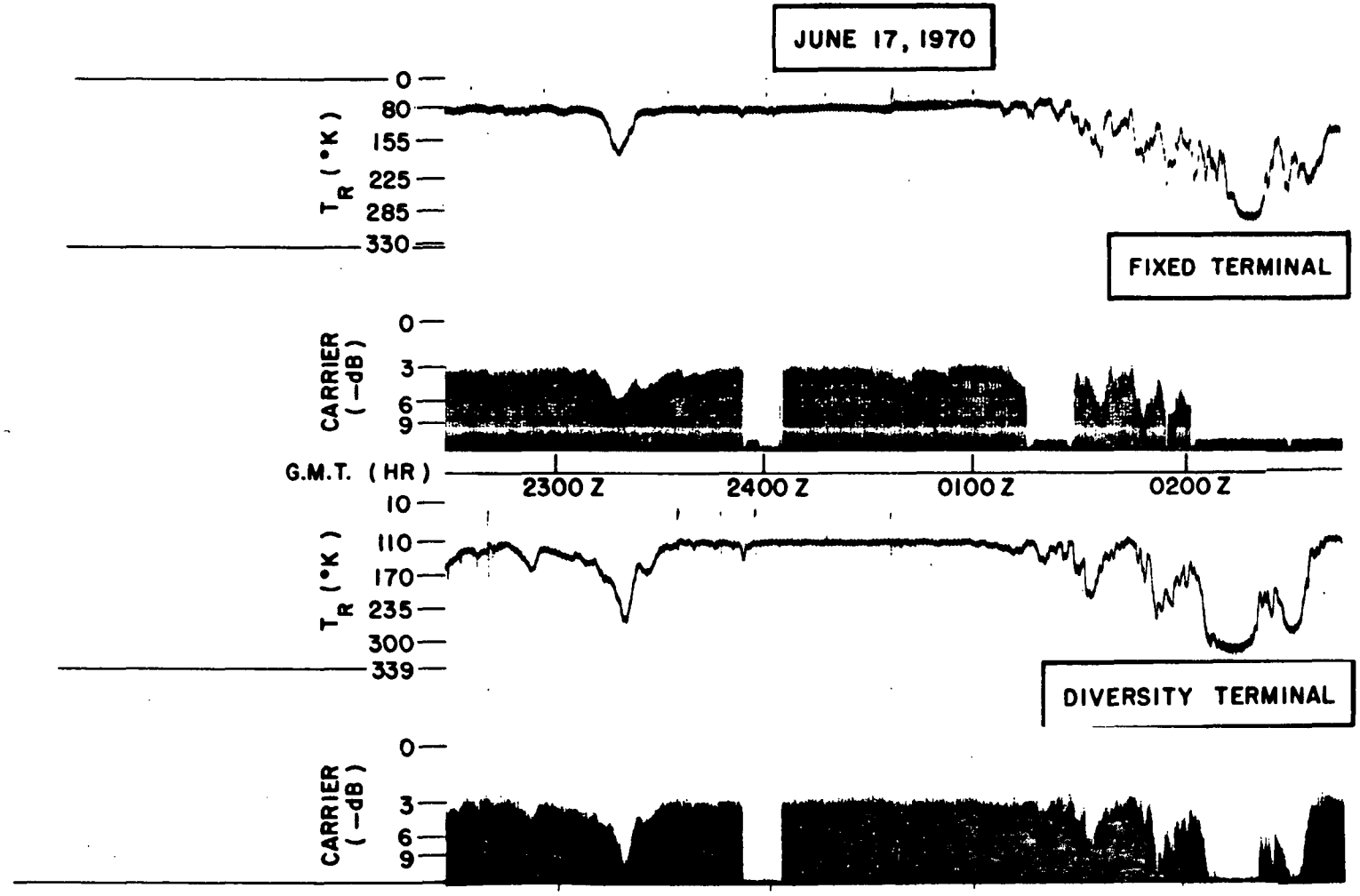

Fig. 5.--Radiometric temperature and received signal level during two site test run 6 on June 17, 1970, (d168). (Fade periods 3 and 4)

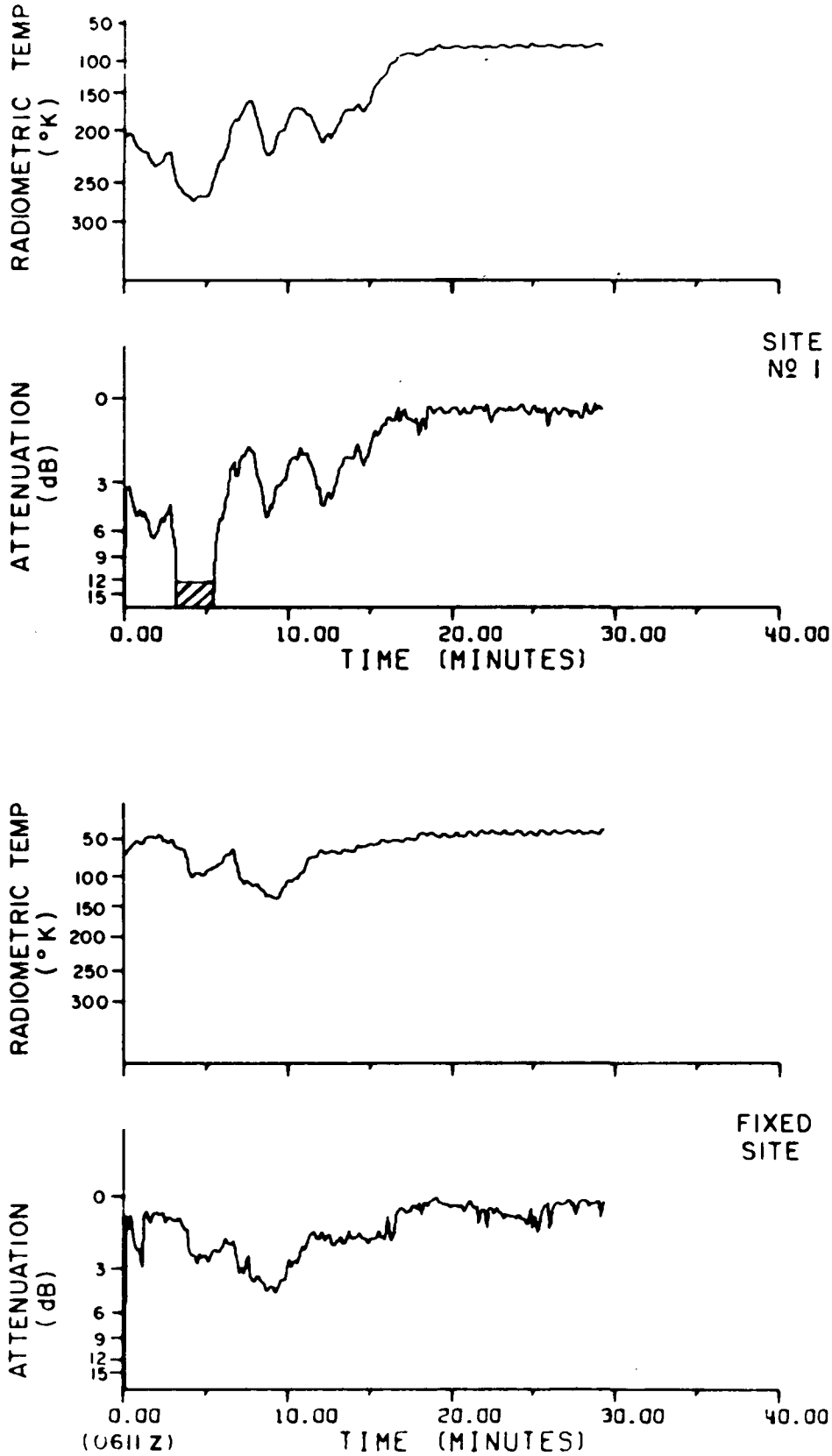

Fig. 6a.--Diversity fade period 1 recorded June 15, 1970.

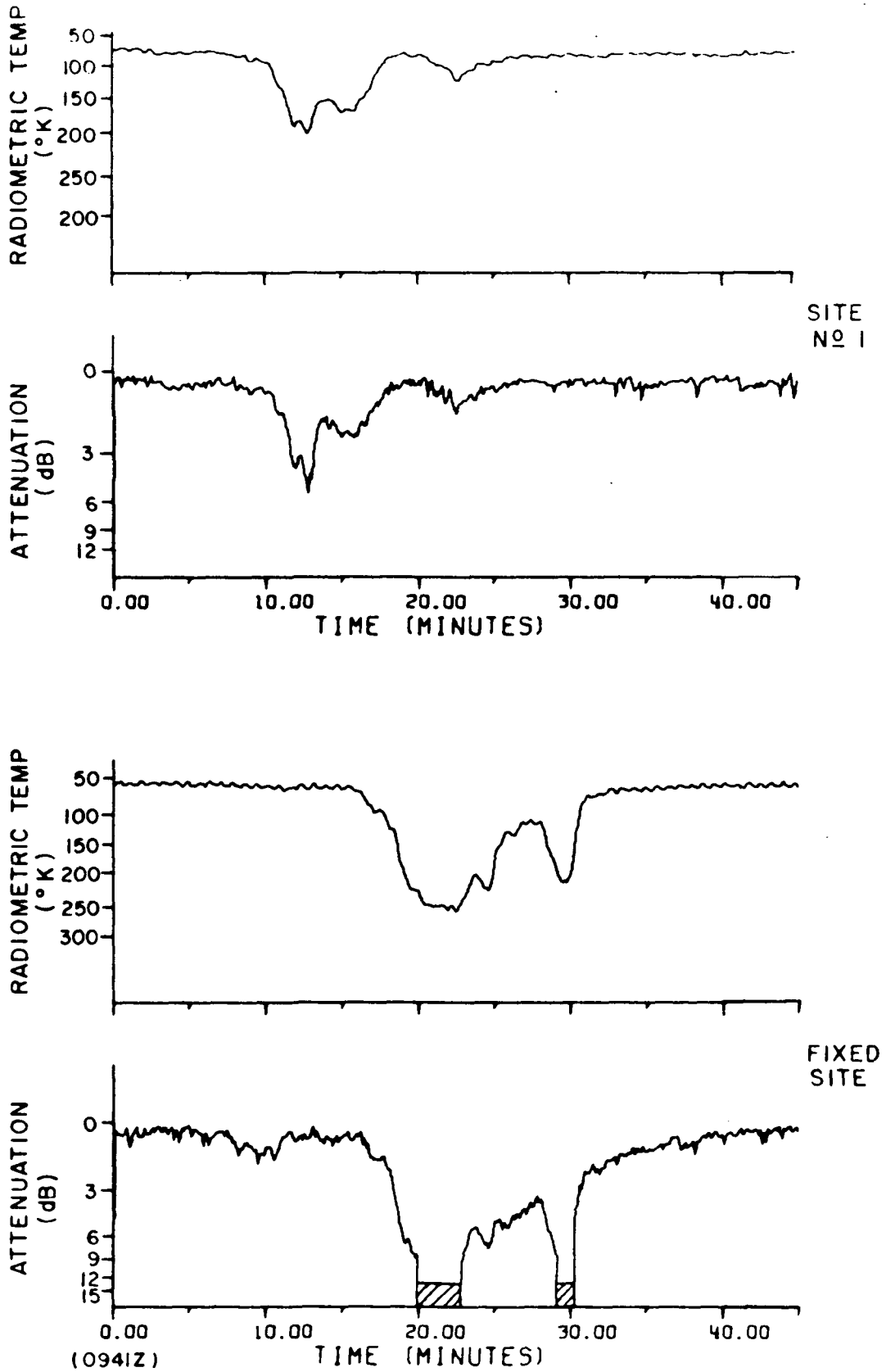

Fig. 6b.--Diversity fade period 2 recorded June 15, 1970.

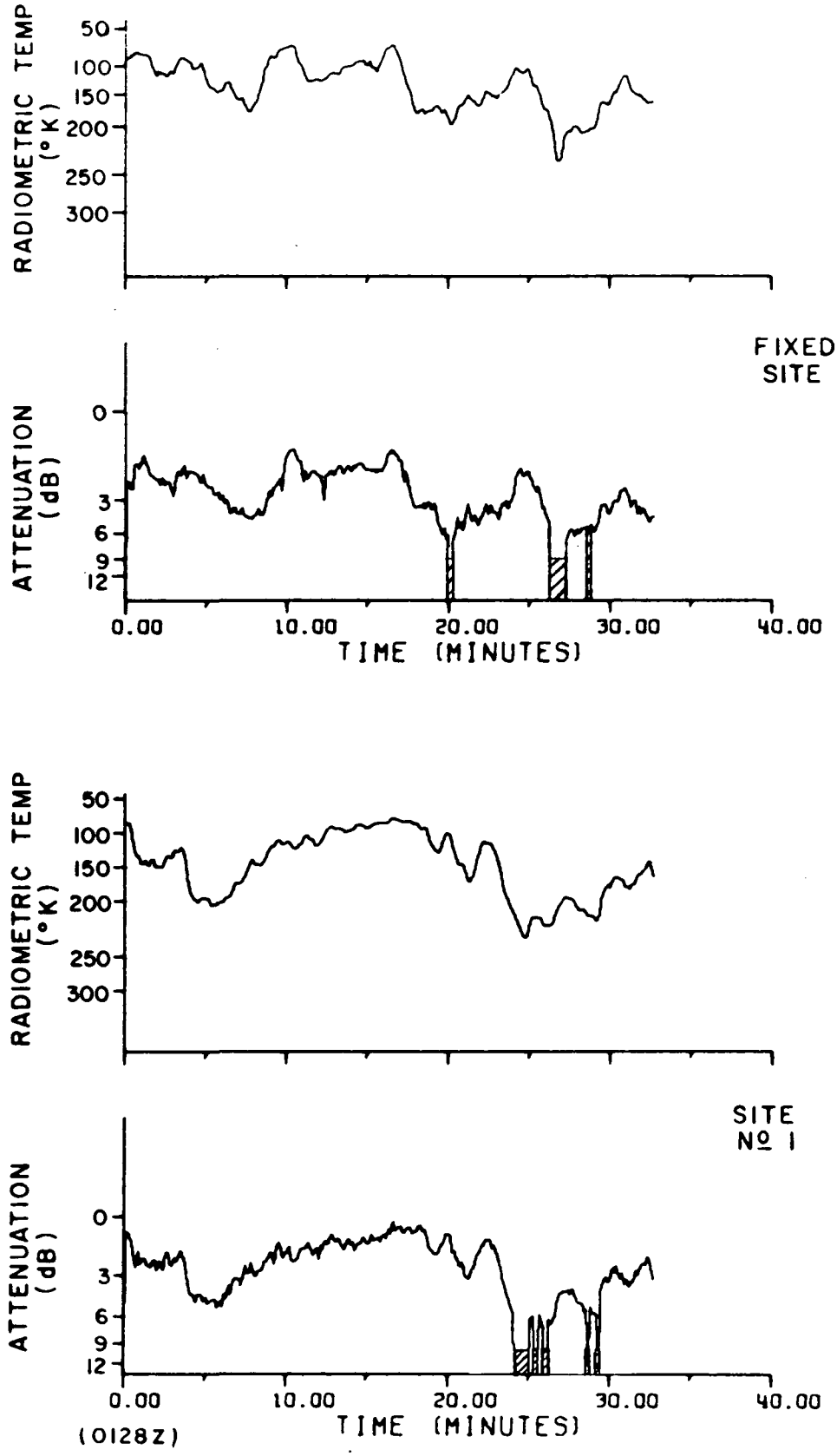

Fig. 6c.--Diversity fade period 4 recorded June 17, 1970.

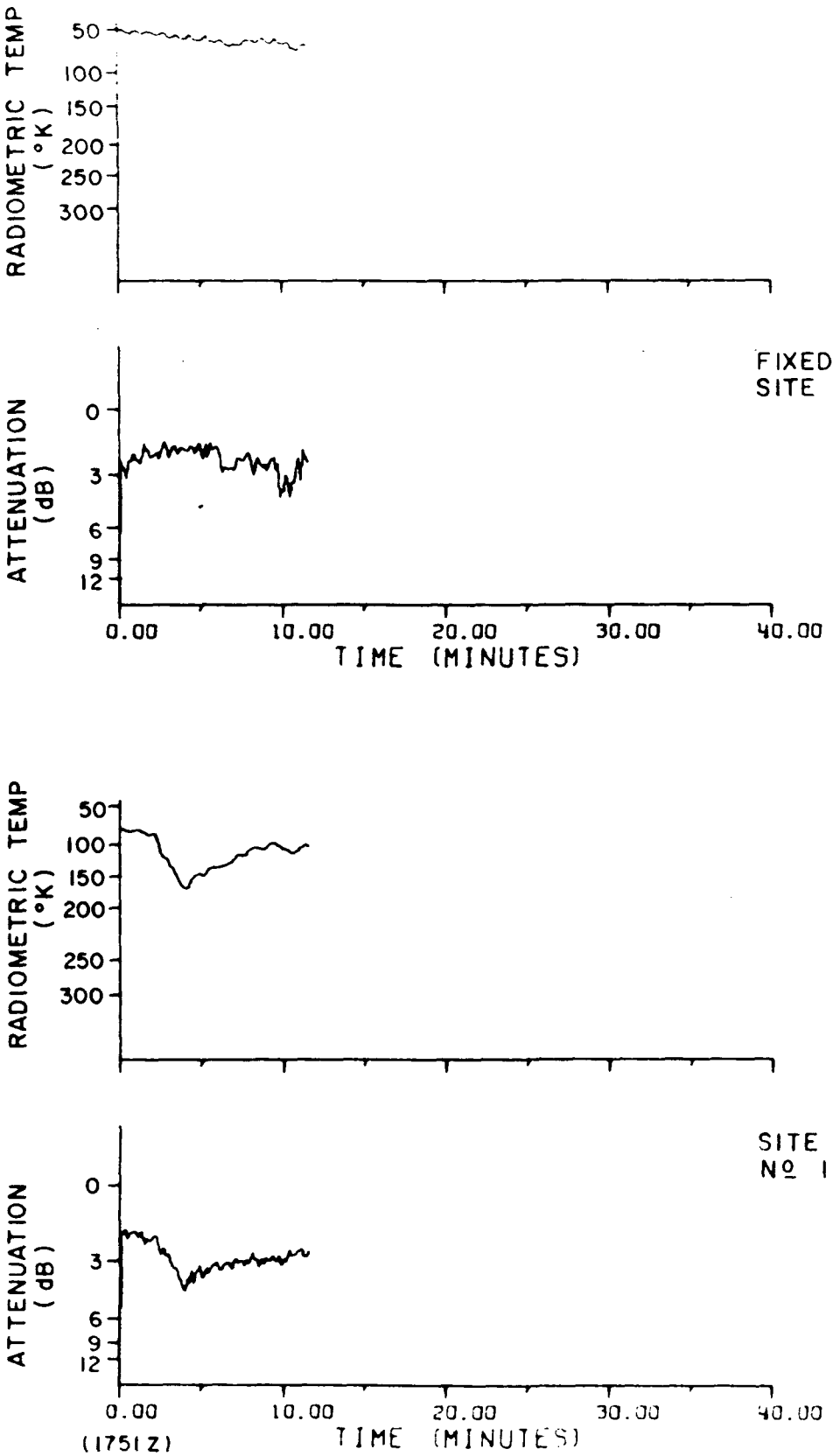

Fig. 6d.--Diversity fade period 5 recorded July 8, 1970.

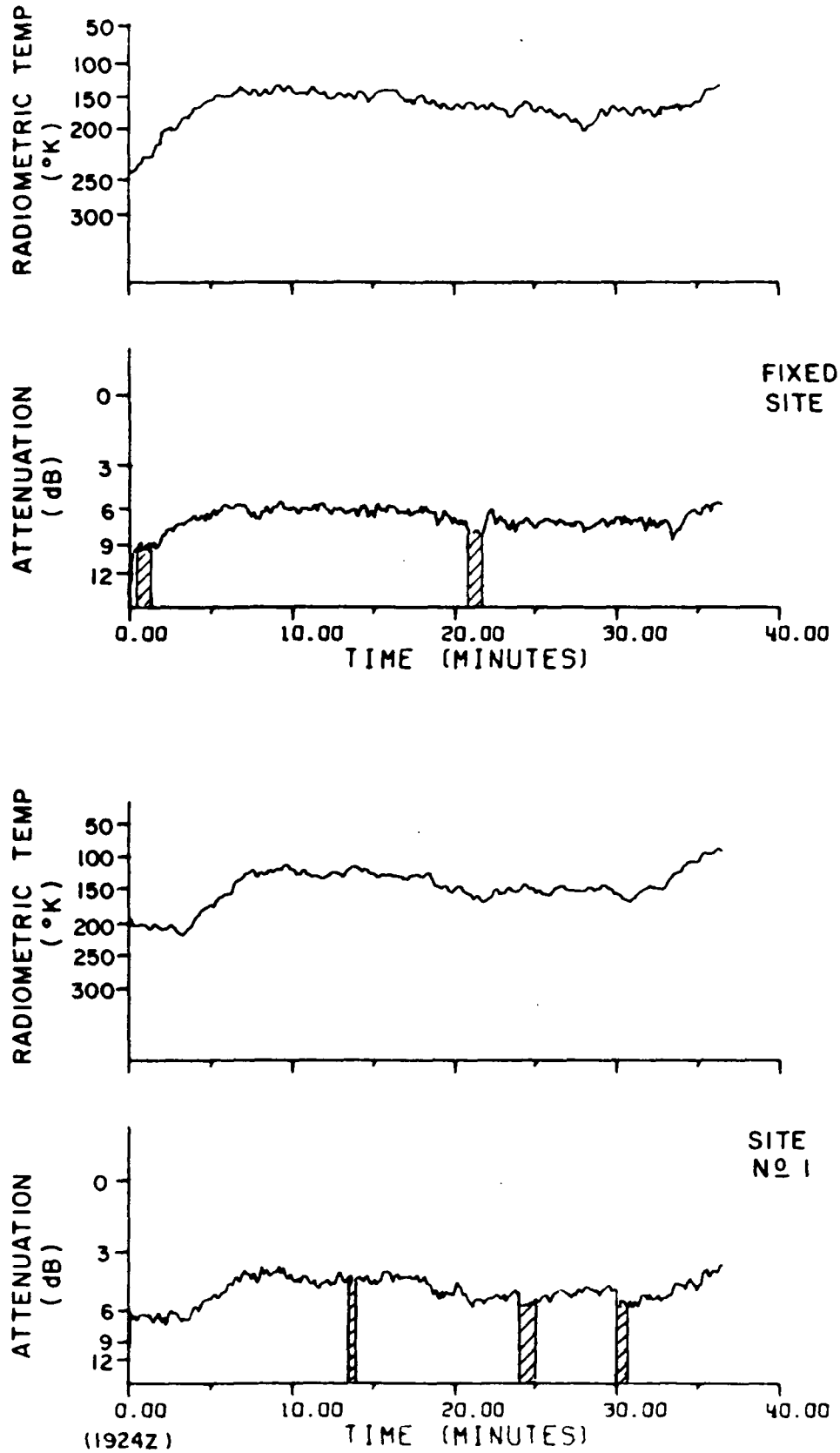

Fig. 6e.--Diversity fade period 6 recorded July 8, 1970.

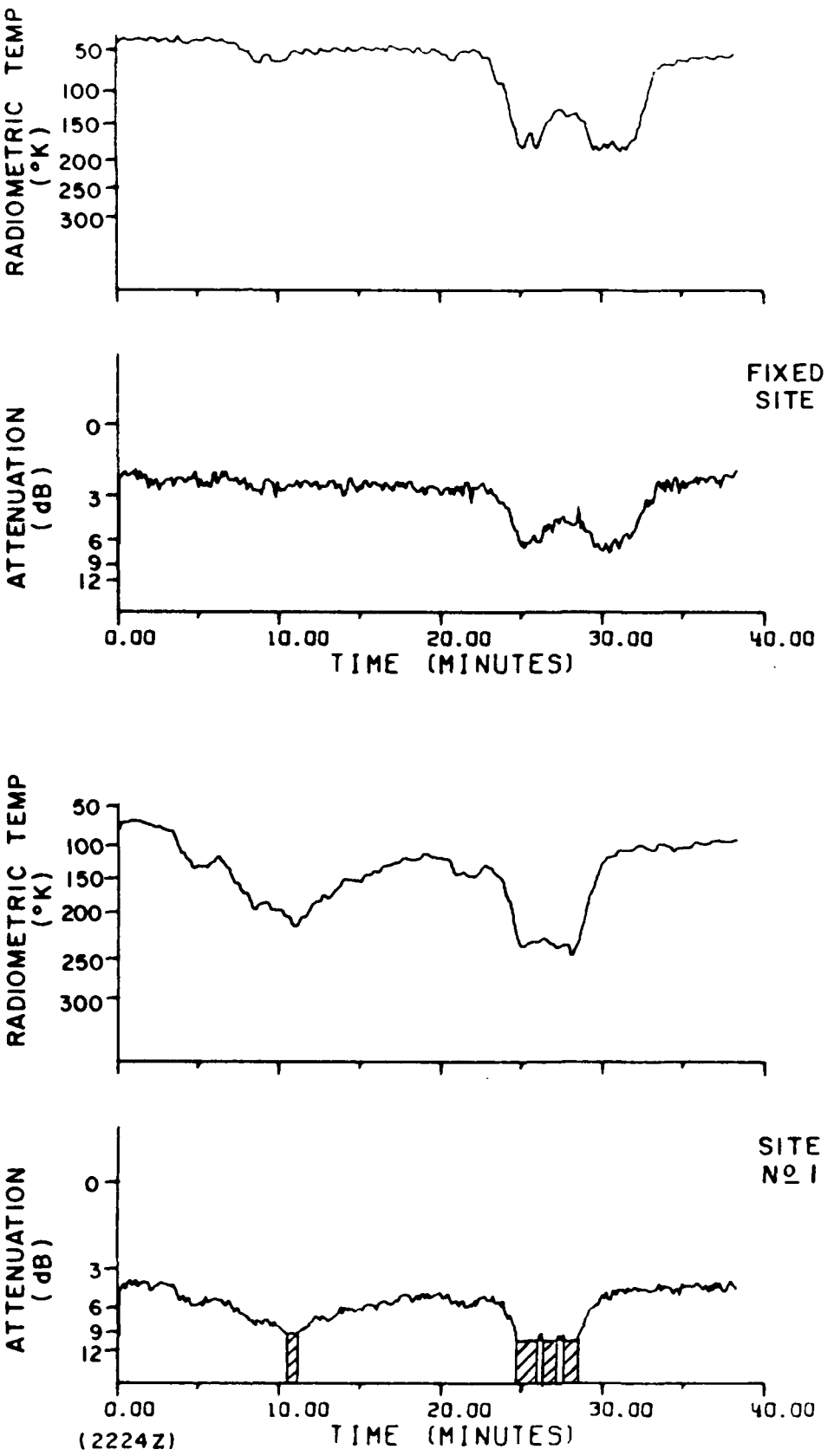

Fig. 6f.--Diversity fade period 7 recorded July 15, 1970.

B. Factors Influencing Data Interpretation

The signal level received from the ATS-5 satellite is influenced by several factors in addition to precipitation attenuation. These are:

(1) Attenuation by atmospheric gases and clouds,

(2) tracking errors due to operator inability to adequately maintain the correct antenna pointing angle or due to gusty winds which cause antenna buffeting,

(3) variations in spacecraft and ground terminal equipment resulting in received signal level changes, and

(4) diurnal variations in the spacecraft orientation relative to the ground terminal.

It has been determined that the diurnal signal variation is due to a small tilt in the spin axis orientation of the spacecraft with respect to the plane of its orbit. This deviation produces an apparent reduction in the spacecraft radiated power which follows an approximate cosine variation during each revolution. Available data on the spacecraft attitude permits a prediction of this diurnal signal variation.

Tracking errors are minimized by developing efficient manual antenna repositioning techniques. However, difficulties in maintaining proper antenna pointing angles even when using the best manual techniques produce an uncertainty in measured attenuation of approximately 0.5 dB. Gain variations due to equipment performance were negligible during the durations of the 1970 two-site fade periods analyzed.

The precipitation attenuation was determined by comparing the attenuated signal level with the nearest-in-time previous clear weather signal level. In this manner the uncertainties in link parameters, e.g., ground terminal antenna gain, atmospheric gas attenuation, spacecraft power variations, etc., do not appreciably affect the analysis. It is thus assumed explicitly that the clear weather signal level, once determined, is invariant during the duration of that fade period.

A PLL receiver calibration was performed during each test run. This calibration procedure consisted of inserting a known 15.3 GHz cw signal level into the front end of the receiving system and recording the dc receiver output. Using this procedure the measured signal detection threshold was approximately -145 dBm. However, the receiver threshold for the ATS-5 pulsed signal was generally much higher and corresponded to a fade margin ranging from 12 to 15 dB. This is due to the inability of the receiver phase lock loop to adequately track highly attenuated signals during the short duration of the received pulses from the spinning satellite. A complete description of satellite spin effects on terminal equipment performance and the resulting propagation measurements may be found in Reference [27].

C. Data Processing

The initial step in the diversity analysis was the A/D conversion of the following analog magnetic tape data channels:

(1) the voltage output of the 15.3 GHz receiver,

(2) the voltage output of the 15.3 GHz radiometer, and

(3) the square wave time signal voltage with one-half second period.

This A/D conversion process accepted analog waveforms with amplitudes in the range 0-5 volts and these waveforms were sampled at the rate of 1,000 samples per second per channel when the analog data was played back at four times the record rate. Consequently, the real time sampling rate was 250 samples per second for each data channel converted. After A/D conversion the third channel was tested to determine the starting point of each time pulse. Whenever a new pulse was encountered a clock index was incremented to indicate the number of half seconds into the test run. The receiver output, the radiometer output, and the clock index were buffered simultaneously when a received signal pulse peak was detected. The digital output to magnetic tape consisted of logic records of 128 sixteen-bit words per channel. The control for this A/D function and peak detection was provided by a HP-2115A computer.

The subsequent editing and data analysis was performed on an IBM 360-75 computer. The edit function was designed to select pertinent sections of a particular test run and to eliminate undesired data samples which arose during the A/D process when multiple detection of a single received pulse occurred. A sample of a received pulse which will result in multiple detection is shown in Fig. 7. This figure is a high speed chart recording of several pulses received at the transportable terminal which shows a local maximum occurring

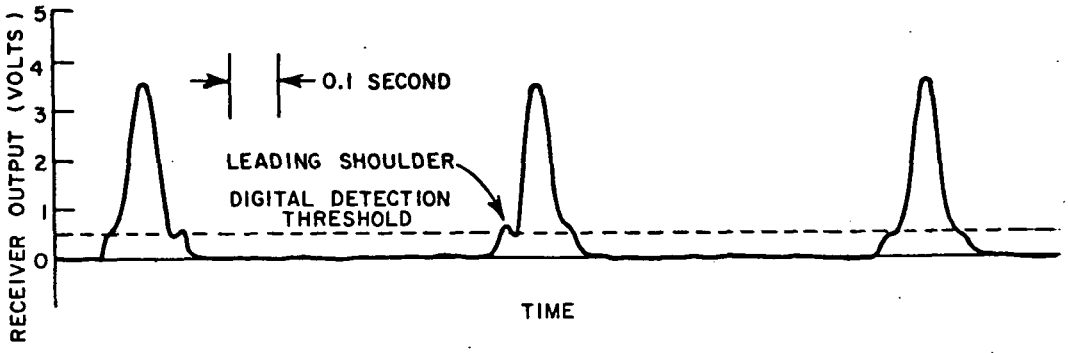

Fig. 7.--High speed recording of received signal.

on the leading edge of one of the received pulses. If the local maximum was greater than the digital detection threshold (usually about 0.5 volt), then both the shoulder and the main pulse peak were treated as pulse peaks during the A/D conversion process. Consequently, preprocessing of the digital data was necessary in order to eliminate these unwanted samples. The final data analysis included the calculation of:

(1) the single- and two-site attenuation distributions,

(2) the conditional attenuation distributions,

(3) the cross-correlation of the received signal levels,

(4) the cross-correlation of radiometric temperature with attenuation at each site,

(5) the distribution of fade durations, and

(6) the mean absorption temperature based on measured attenuation and radiometric temperature.

CHAPTER V
EXPERIMENTAL RESULTS

A. Attenuation Distribution

The measured single- and two-site fade distributions relative to the clear weather levels for each of the seven diversity fade periods are shown in Fig. 8. Curves indicating the time interval during which the received signals at both terminals were simultaneously below a given level are also shown for each case. The attenuation distribution data for all seven periods are replotted as a cumulative distribution in Fig. 9. Here the percentage of the total measurement period (270 min.) is listed on the ordinate. The 6 dB attenuation level was exceeded 7.05% of the measurement period at the transportable terminal and 8.36% at the fixed terminal, while both terminals were simultaneously at or below the 6 dB level only 0.87% of the time. Two-site diversity operation with a 4 km separation was effective in reducing the cumulative measured attenuation durations of fades greater than 6 dB by at least an order of magnitude. Figure 9 may also be interpreted in another way. The best cumulative single site performance during thunderstorm rain periods in June and July, 1970, resulted in an outage time of 285 seconds. For this same outage the fade margin for the diversity system could have been reduced from approximately 14 dB to 5.5 dB.

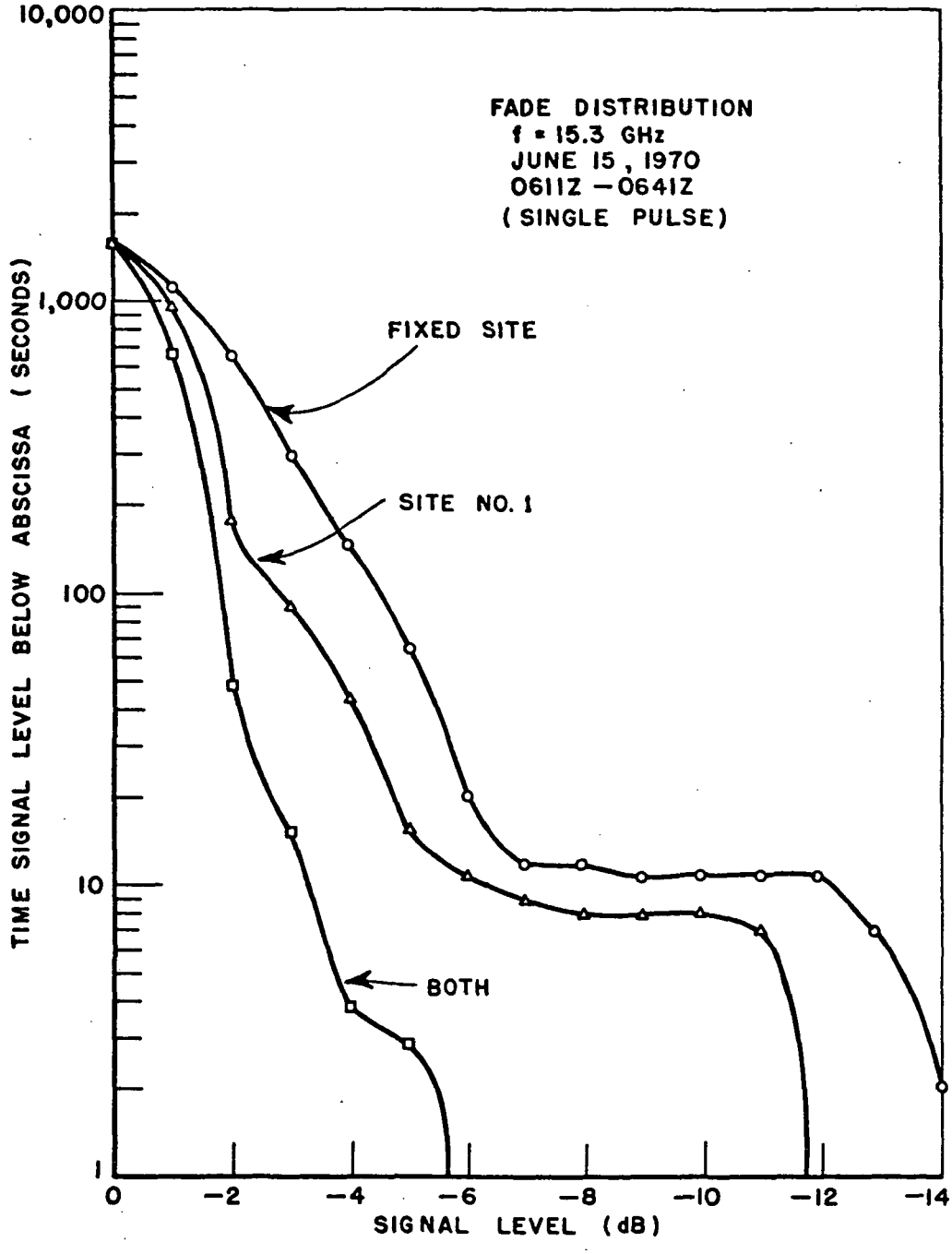

Fig. 8a.--Fade distribution for period 1.

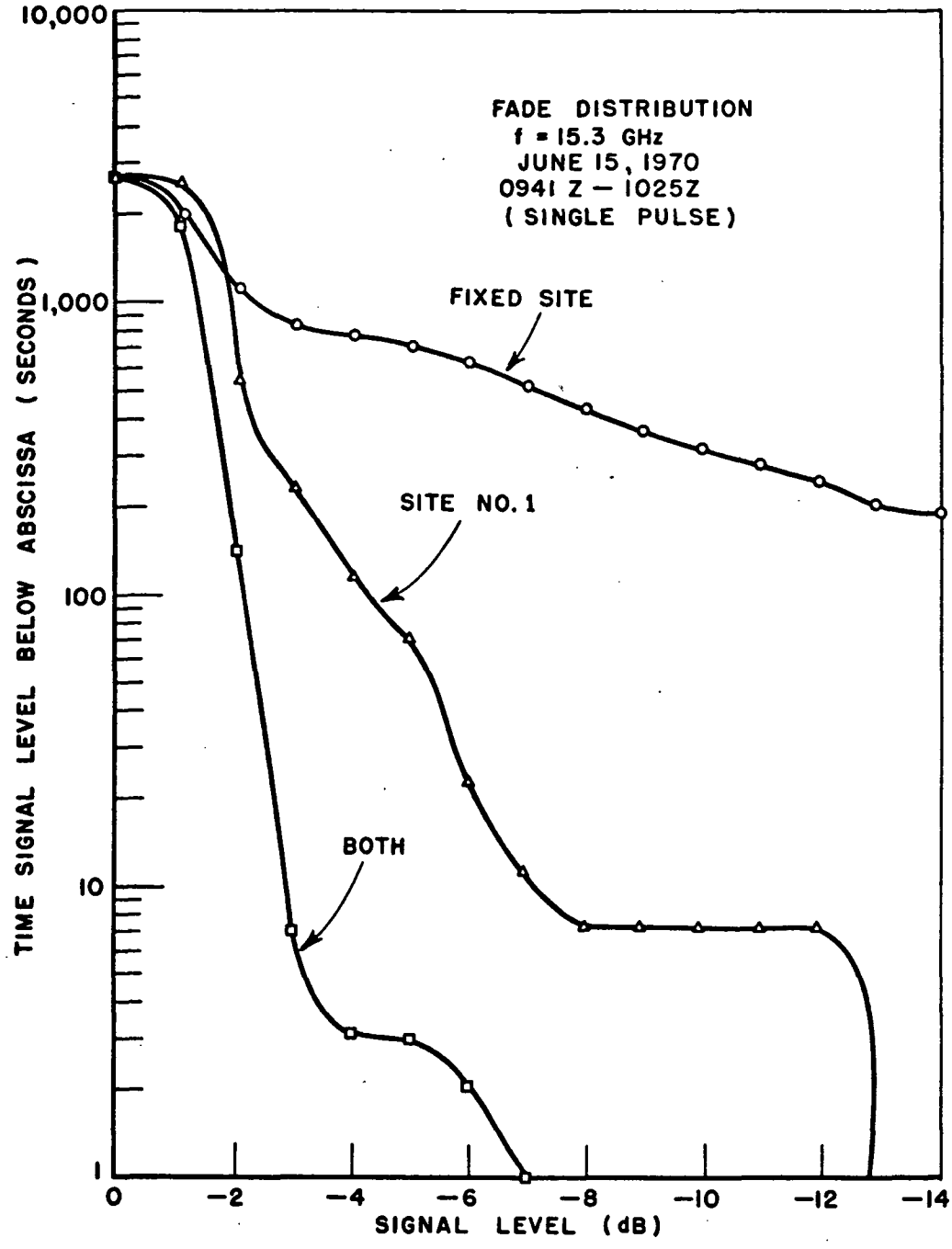

Fig. 8b.--Fade distributions for period 2.

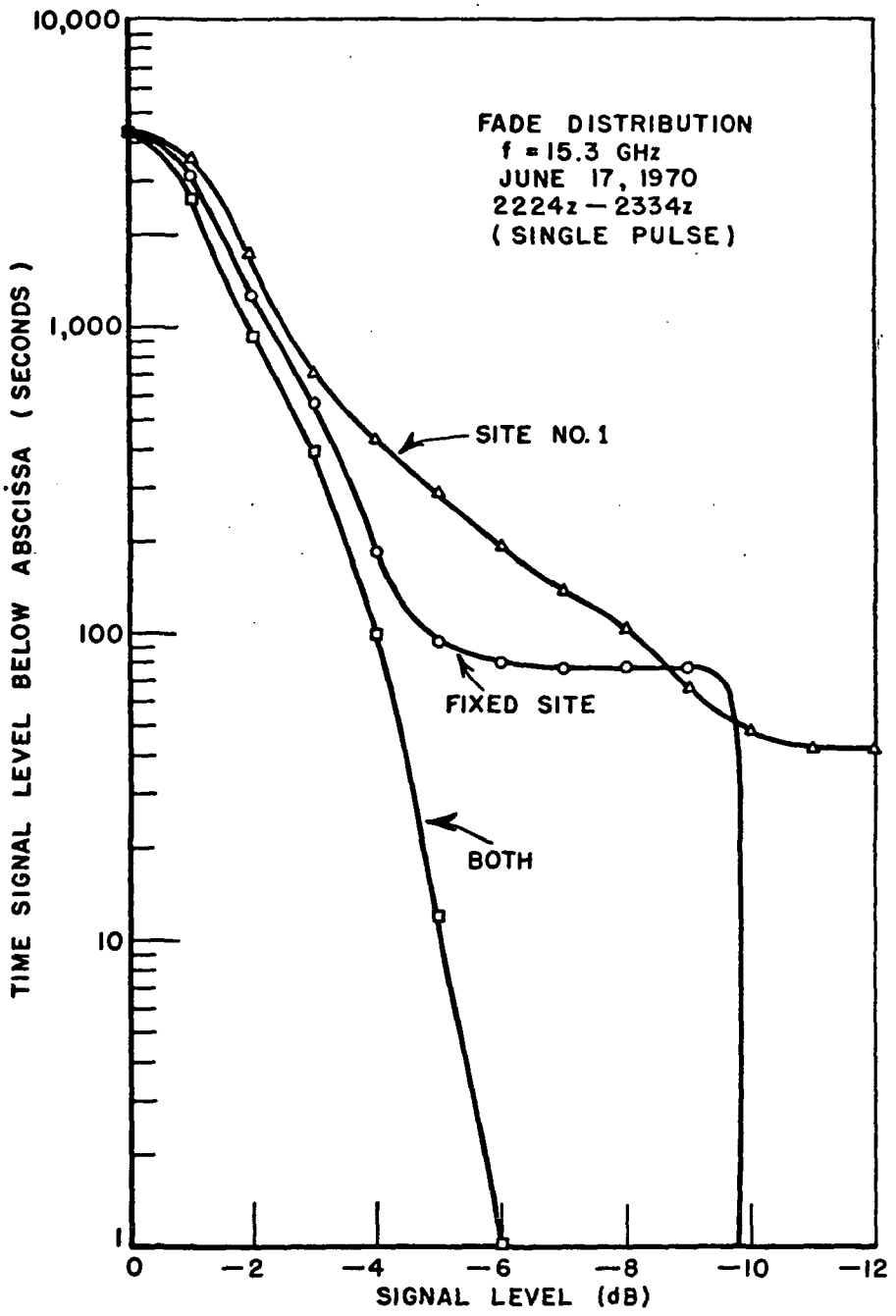

Fig. 8c.--Fade distributions for period 3.

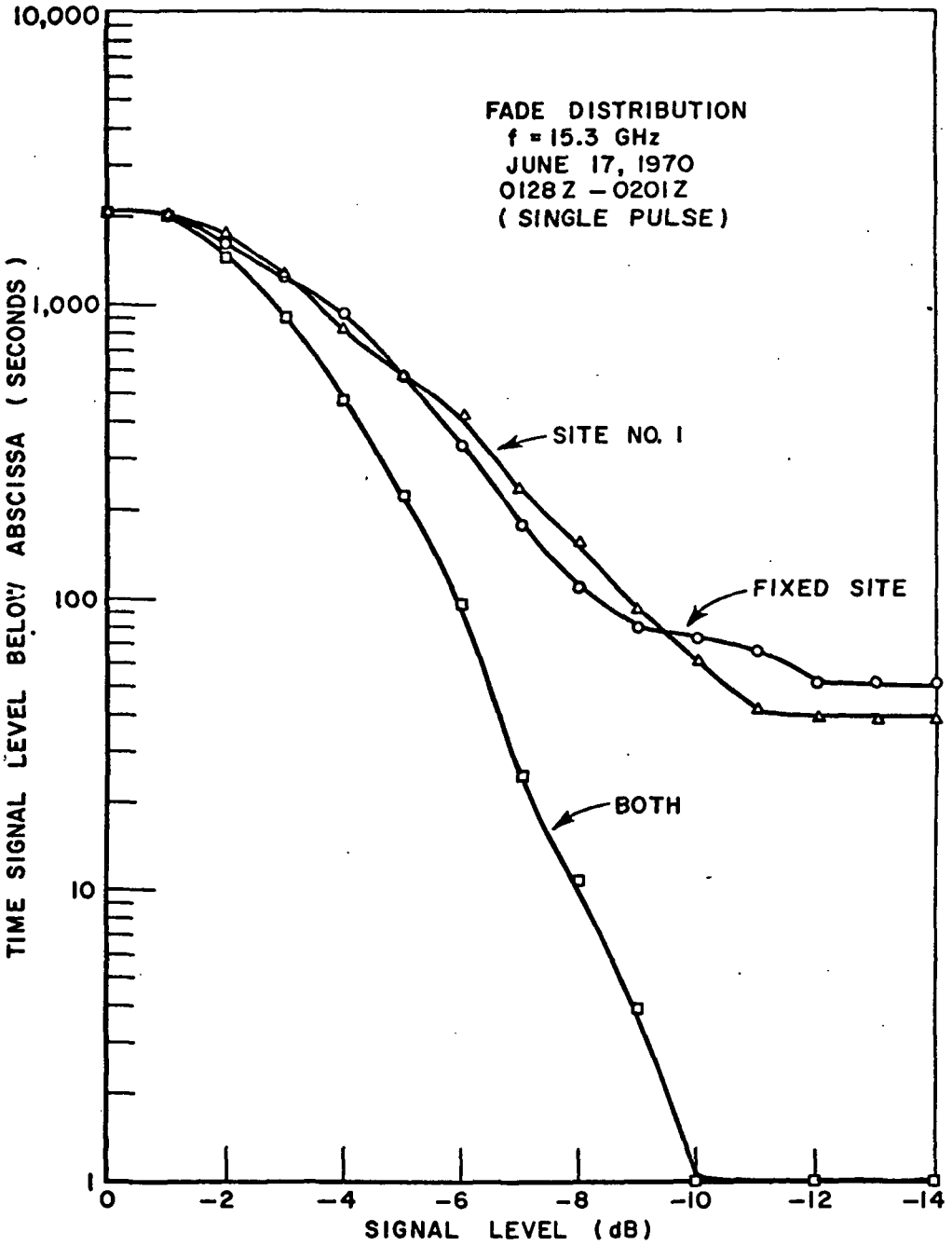

Fig. 8d.--Distributions for period 4.

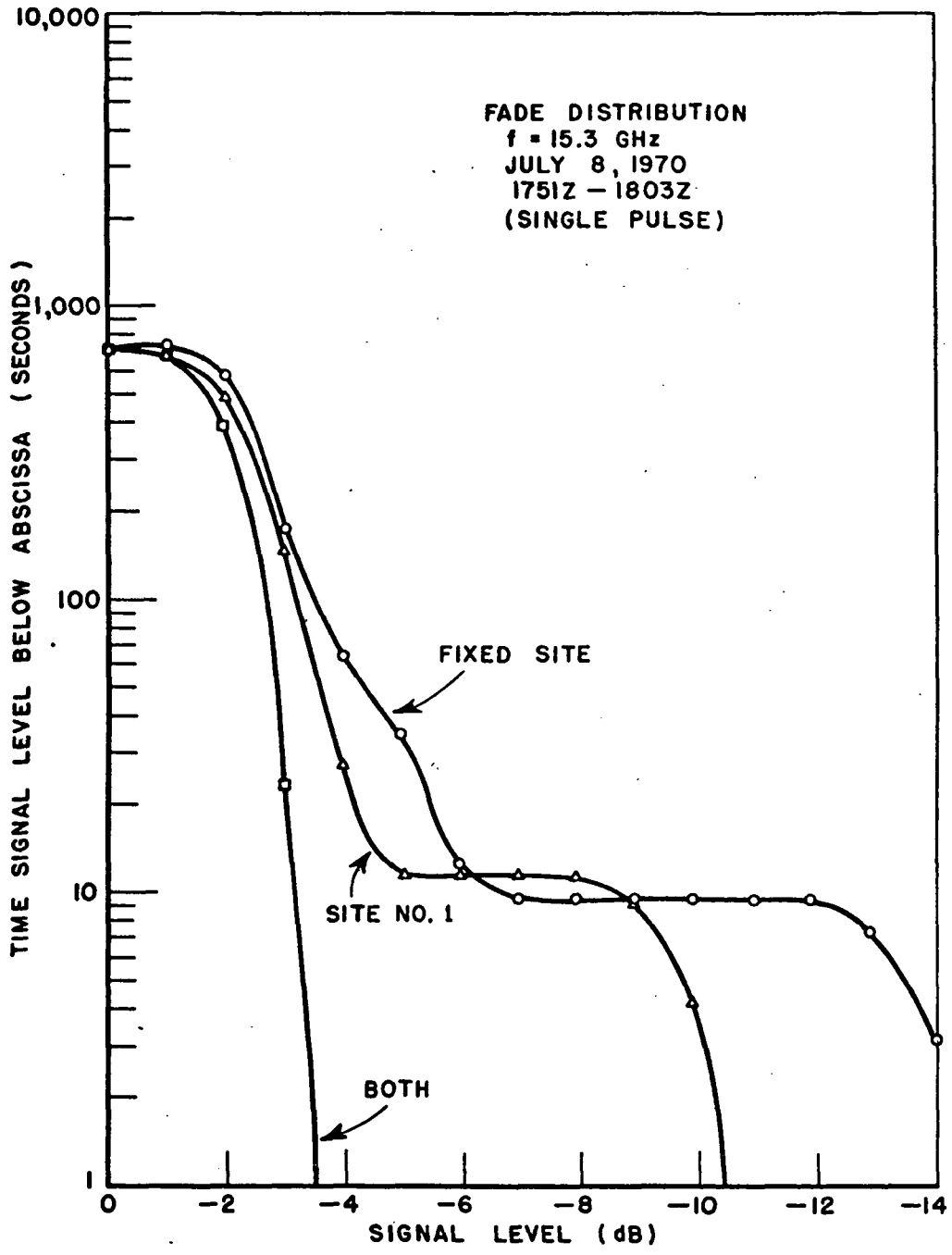

Fig. 8e.--Fade distributions for period 5.

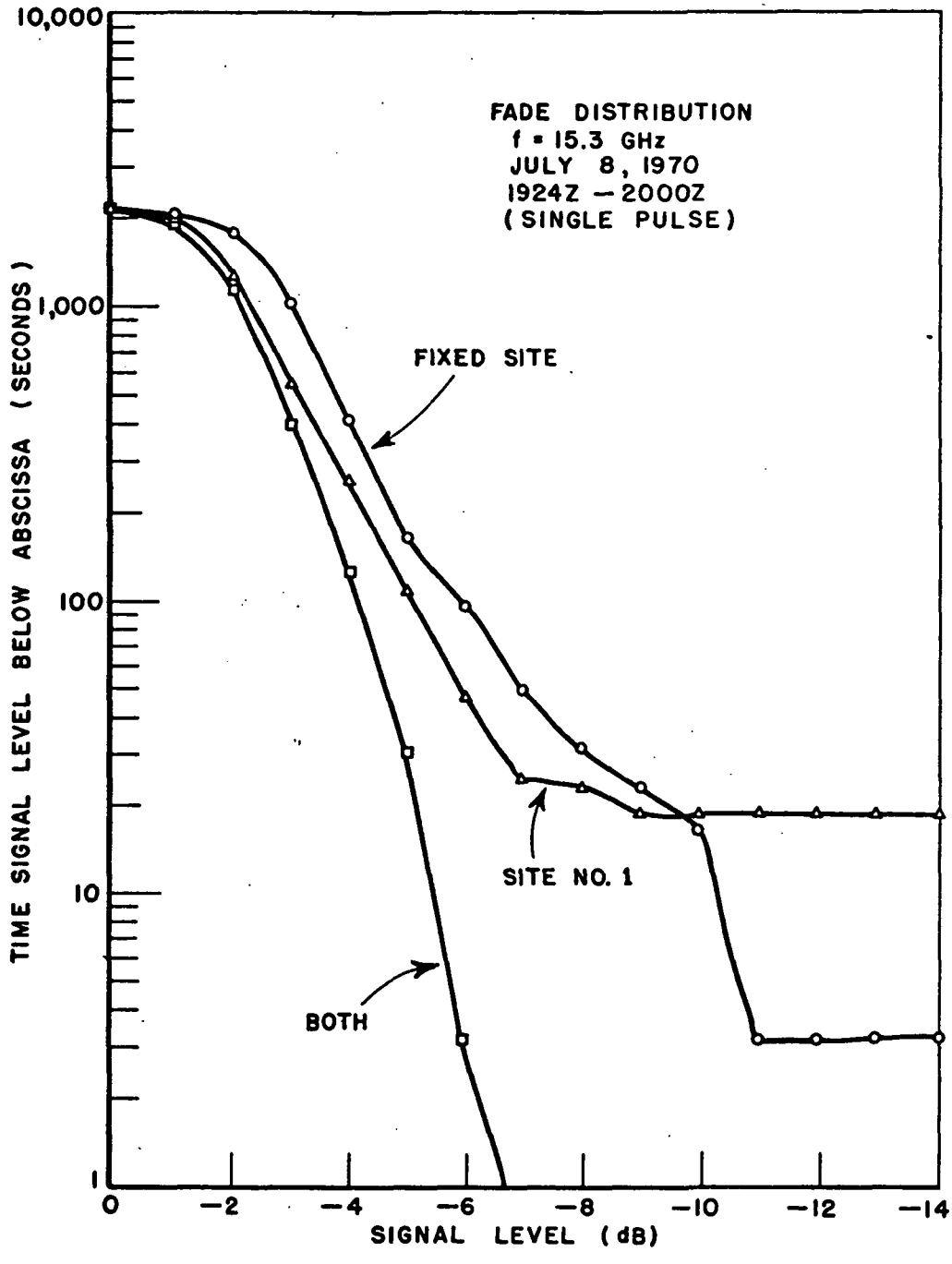

Fig. 8f.--Fade distributions for period 6.

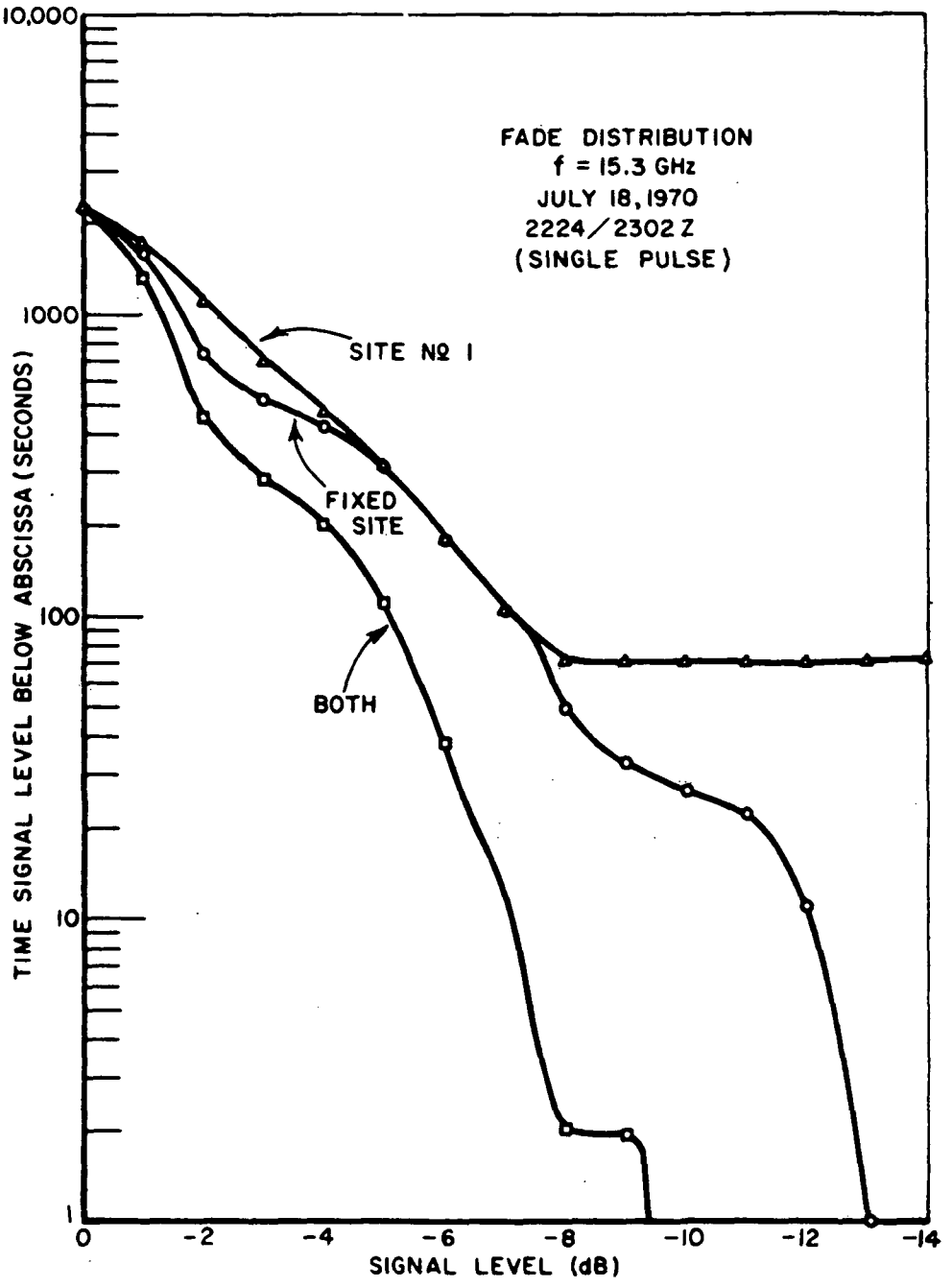

Fig. 8g.--Fade distributions for period 7.

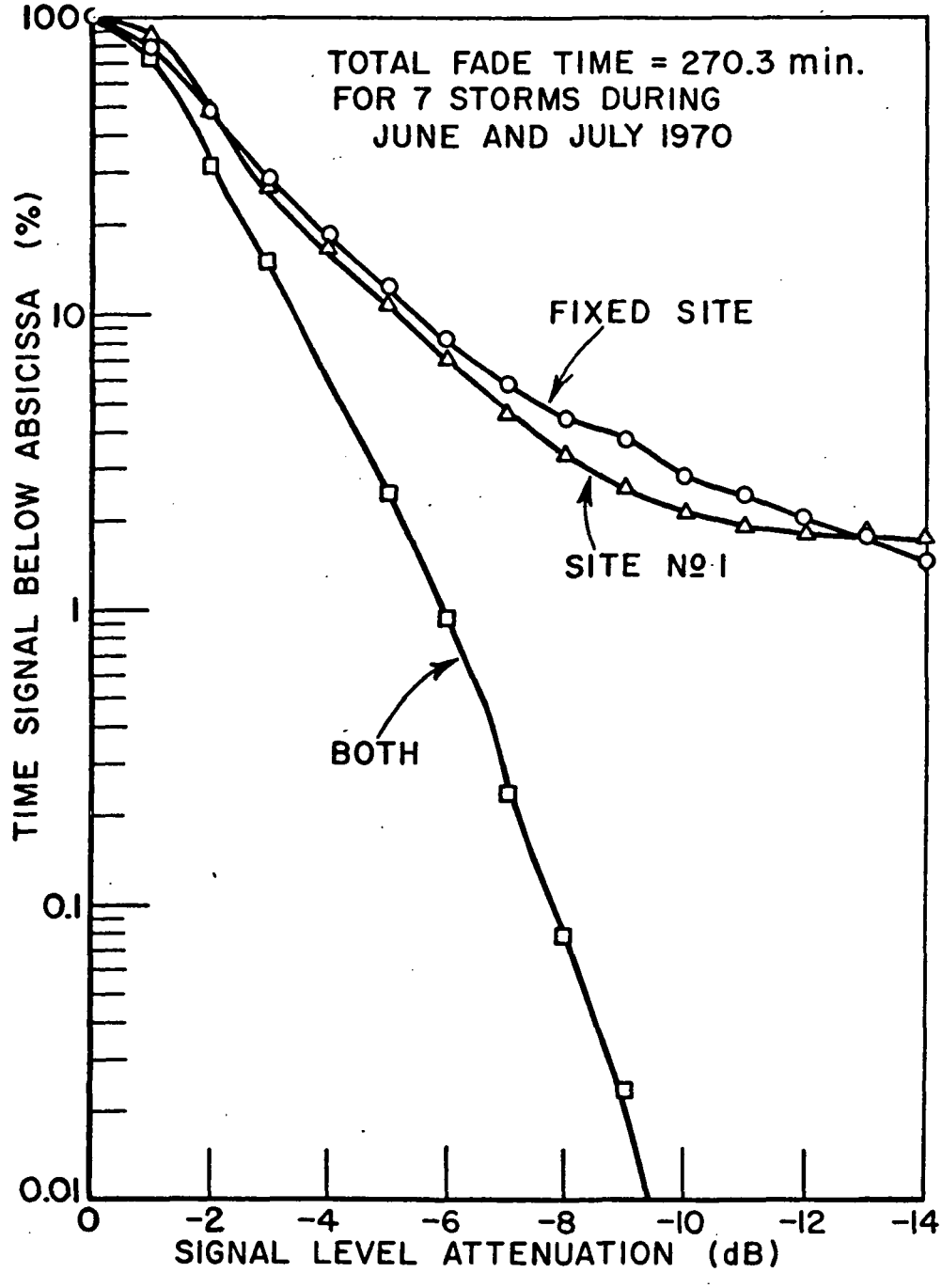

Fig. 9.--Cumulative fade distribution for seven data periods in June and July, 1970.

The data shown in Fig. 9 are based on 4.5 hours of measured attenuation data. This corresponds to 0.31% of the time in the months of June and July, 1970. Based on tipping bucket measurements continuously made at the fixed site during these months, the clock hourly rain rate exceeded 6.6 mm/hr for 0.75% of these two months. This rate is associated with rain of moderate intensity, and rates exceeding this value will typically produce attenuations of significant levels. Consequently, the attenuation data extends over approximately 41% of the time when at least moderate to heavy rain was observed at the fixed site during June and July, 1970. The adequacy of this sample for describing the propagation characteristics is substantiated in a sense by the similarity of the single-site cumulative distribution curves. This indicates that the two-terminal distribution has not been biased by a disproportional amount of intense rain at one of the sites.

Statistics compiled by the U.S. Weather Bureau for the period 1904-1943 show that the largest percentage of thunderstorm days has occurred during the months of June and July in Columbus, Ohio (20.3% and 20.9%, respectively, of the total storm days in the period).[28] Storms during these months generally produce high rain rates for short durations as compared with the less intense, longer duration rainfalls which occur during other times of the year. Thus the attenuation distribution curves in Fig. 9 are considered representative of single- and two-terminal performance during the worst expected conditions of fading due to precipitation attenuation on satellite-to-ground millimeter wave paths terminating in the central Ohio region.

B. Correlation of Attenuation Between the Two Sites

The cross-correlation function of the attenuated signals received at both sites during each of the measured rain periods in June and July, 1970, has been computed. These cross-correlation functions, which were computed for various time lags of the fixed site signal level with respect to the transportable site signal level, yield information on thunderstorm cell size, structure, and motion as the cell progresses through the propagation paths. Although the rigorous interpretation of these cross-correlation functions may be debated, they do provide an explicit means of comparing the fading structures and the fade time delays of the received signals at the two sites. Thus, the cross-correlation coefficient implicitly describes the change in the thunderstorm cell structure and the speed of the cell as it crosses the propagation paths.

For these purposes the cross-correlation function may be written as

$$(13) \qquad \rho_{xy}(\tau) = \frac{\frac{1}{N}\sum_{i=1}^{N}[(x(t_i+\tau)-\bar{x})(y(t_i)-\bar{y})]}{[\frac{1}{N}\sum_{i=1}^{N}(x(t_i+\tau)-\bar{x})^2 \frac{1}{N}\sum_{i=1}^{N}(y(t_i)-\bar{y})^2]^{1/2}} .$$

Equation (13) may be used to compute the cross-correlation function of the measured attenuations if the following variable assignments are made:

$x(t_i)$ = the peak pulse received signal at the transportable terminal at time t_i,

$y(t_i)$ = the peak pulse received signal at the fixed terminal at time t_i,

N = the number of pulses in the fade period,

τ = the time delay with respect to the received signal at the transportable site,

$\bar{x}$ = the time average peak pulse received signal at the transportable terminal, and

$\bar{y}$ = the time average peak pulse received signal at the fixed terminal.

In order to simplify the computational procedure the pulse amplitude records were defined to be periodic in time with period equal to the duration of the fade period under consideration. Then Eq. (13) reduces to

$$(14) \qquad \rho(\tau) = \frac{\frac{1}{N}\sum_{i=1}^{N} x(t_i+\tau)\, y(t_i) - \bar{x}\,\bar{y}}{\left[\frac{1}{N}\sum_{i=1}^{N} (x^2(t_i)-\bar{x}^2)\,\frac{1}{N}\sum_{i=1}^{\infty} (y^2(t_i)-\bar{y}^2)\right]^{1/2}} \quad .$$

This arbitrary definition of periodicity also implies that the values of the cross-correlation function computed for delay times greater than half the duration of the fade period will be physically meaningless. During periods when the received signal was below the receiver threshold, the received pulse amplitude was arbitrarily defined to be the minimum detectable level for computational purposes.

The cross-correlation function for the fading carrier signals in fade period 1 is shown in Fig. 10. The greatest positive cor-

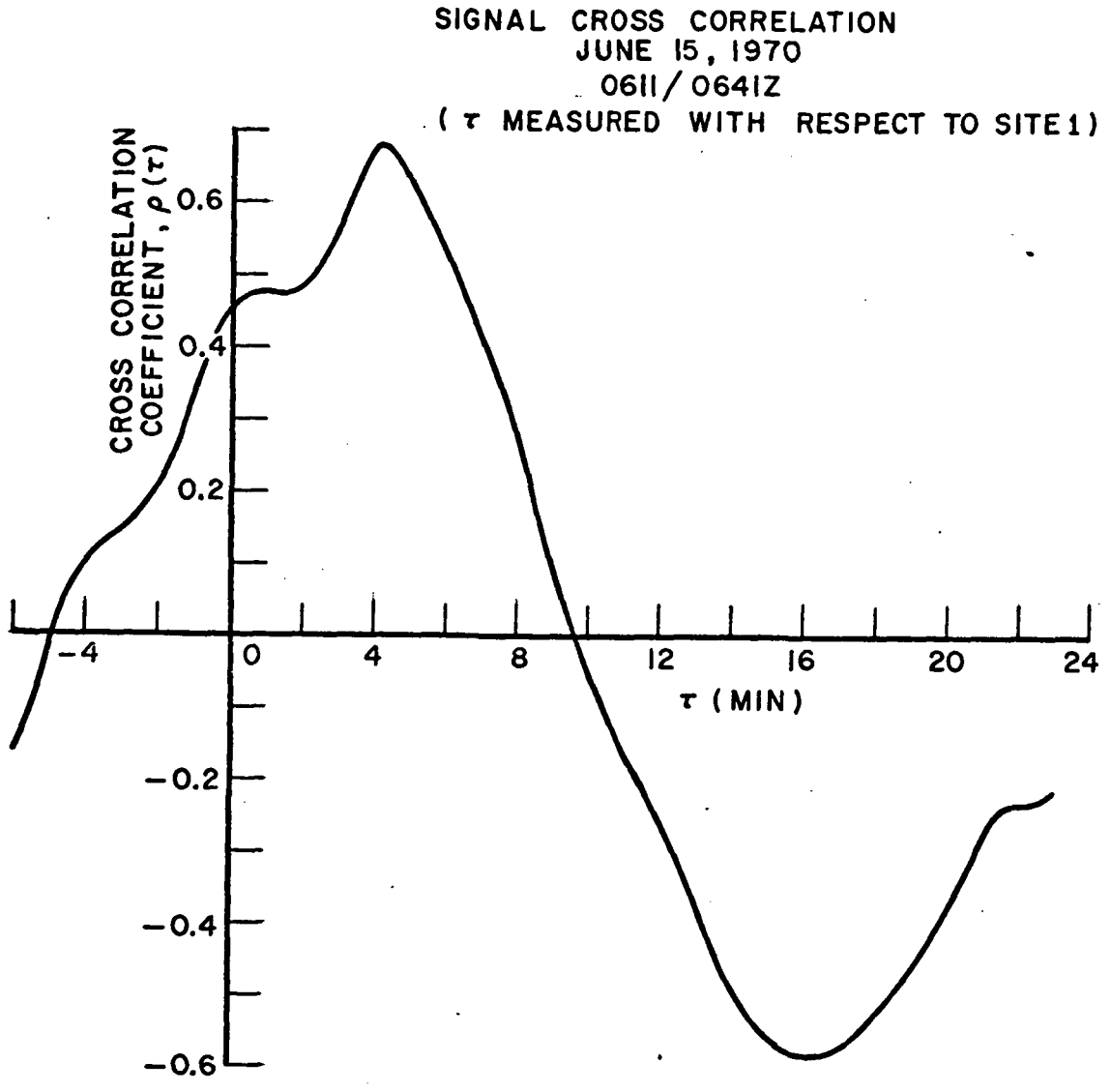

Fig. 10.--Attenuation cross-correlation for period 1.

relation is 0.69 and occurs for a time lag of slightly more than 4 minutes with respect to the transportable terminal. If the thunderstorm cell structure and rain rate do not change as the cell passes through the propagation paths, then this time lag is a simple measure of cell motion. The results shown in Fig. 10 indicate that

the received signals are partially correlated for zero delay, i.e., $\rho(0) = 0.47$. The large negative values for ρ computed for values of τ which are greater than half the duration of the fade period result from the assumed periodicity of the received signals.

The cross-correlation function for the fading signals recorded in period 2 is shown in Fig. 11. The maximum correlation occurs for

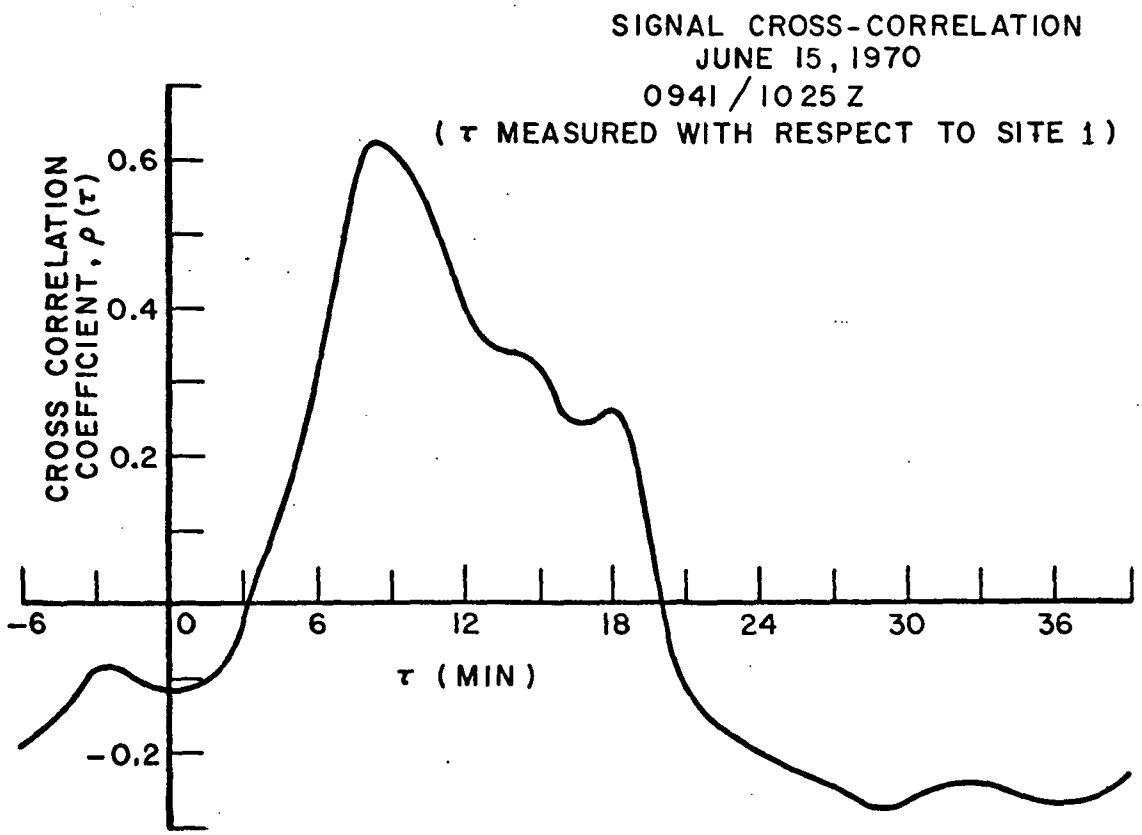

Fig. 11.--Attenuation cross-correlation for period 2.

a delay time of 8 minutes with respect to site 1 ($\rho(8 \text{ min}) = +0.635$). This lag is longer than the duration of all fades at site 1 and longer than the duration of all fades below 5 dB at the fixed site.

However, fade period 2 is rather atypical in that such an intense rain cell does not usually move as slowly as a lag of 8 minutes implies (this lag corresponds to a velocity of 22.5 km/hr perpendicular to the propagation paths).

The results of the attenuation correlation analysis for the seven fade periods are presented in Table 2. Included in this table

TABLE 2

CROSS-CORRELATION OF MEASURED ATTENUATION AT THE TWO SITES DURING JUNE/JULY 1970

PERIOD	DAY	$\rho(\tau=0)$	ρMAX	DELAY, τ
1	166	+.469	+.685	4.0 MIN
2	166	-.128	+.635	8.0
3	168	+.620	+.620	0.0
4	168	+.261	+.420	2.0
5	189	-.112	+.219	3.5
6	189	+.459	+.459	0.0
7	196	+.319	+.470	3.0
Cumulative	June/July 1970	+.452	-	4.1 MIN

are: the cross-correlation coefficient of the undelayed carrier signals, i.e., at $\tau=0$, the maximum of the cross-correlation function, and the value of the delay, τ, associated with the maximum cross-correlation for each period. Note that five of the seven periods produced positive time delays measured with respect to site 1. The average delay associated with these five periods was 4.1 min which corresponds to an average cell velocity of 43.8 km/hr perpendicular to the propagation paths and indicates that the rain events progress in a general west to east direction. These characteristics are in

agreement with typical thunderstorm cell behavior in this region. However, periods 3 and 6 show zero lag from which it may be concluded that both propagation paths were encompassed by the same storm event at the same time and experienced simultaneous maximum fading.

The measured variation of $\rho(0)$ for the seven individual periods was about 0.75 (-0.128 to +0.620). If, however, the seven periods are considered to be a single collection of events having a total period equal to the sum of the durations of the individual periods, then a single cross-correlation coefficient may be computed. This cumulative coefficient of cross-correlation for the data obtained during June and July, 1970, with a 4 km site separation was +0.452. The significance of this result is that it tends to substantiate the initial assumptions regarding the expected spatial rain distributions and indicates that the desired value of cross-correlation, 0.50, was very nearly realized (see Chapter III).

C. Conditional Distribution of Attenuation

The ultimate objective of judicious siting is to minimize the time that one or more rain cells might simultaneously intersect both propagation paths, thereby causing nearly coincident fade events at both terminals. The results of the attenuation correlation analysis presented in the previous section indicate that coincident fading at the two sites is as likely to occur as is noncoincident fading for the 4 km separation distance. The degree to which noncoincident fading occurred at the two sites is shown in Fig. 12. These curves, taken from data collected during period 2, represent the distribution of the measured attenuation at the fixed site with

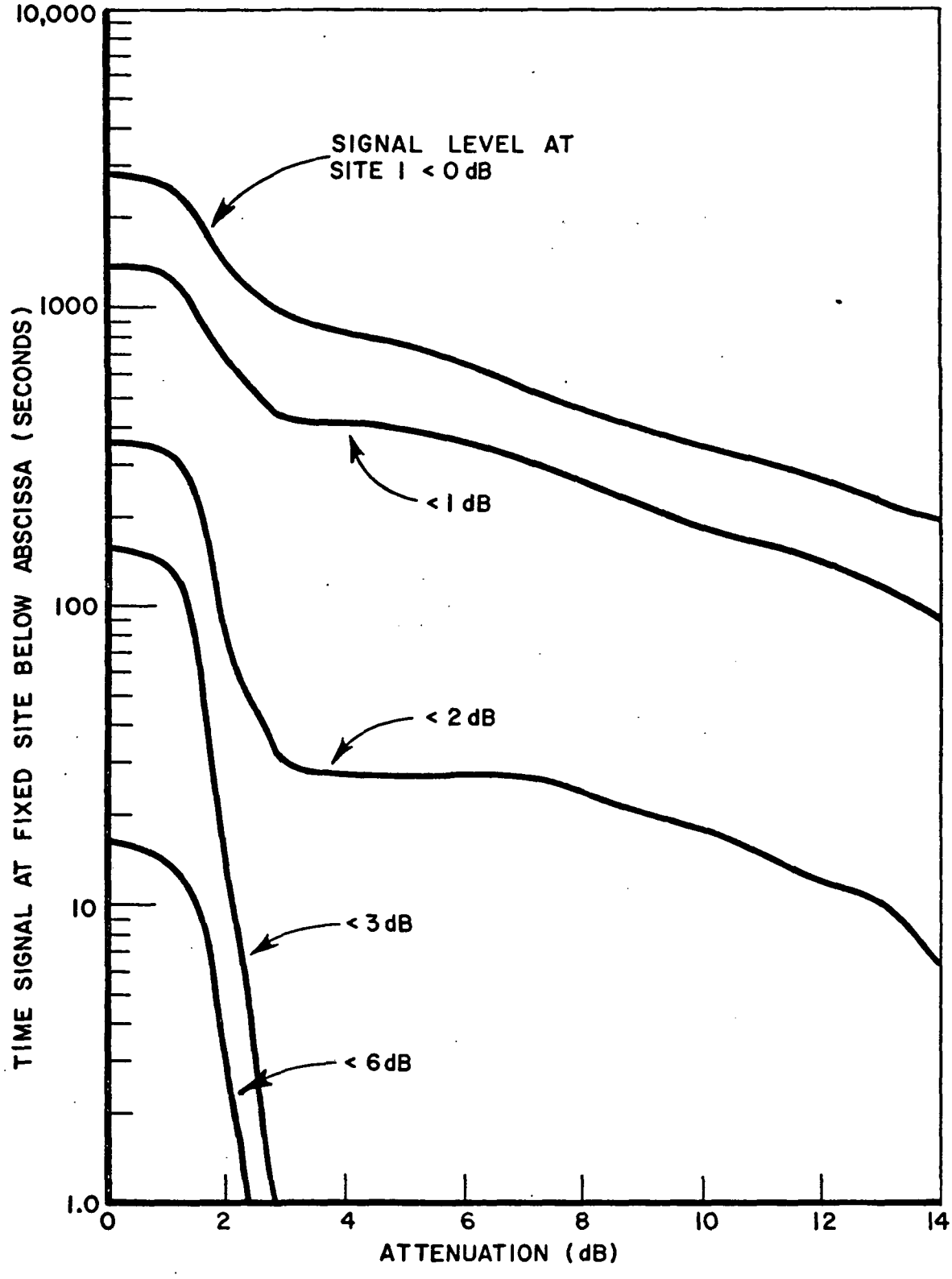

Fig. 12.--Conditional fade distribution for period 2.

the condition that the received signal at site 1 is attenuated below various stated levels. The rain rate accompanying the cell of period 2 was much greater when intersecting the path from the fixed site than at an earlier time when the same cell intersected the path from site 1. Consequently, all of the severe attenuation (below 4 dB) experienced at the fixed site occurred at a time when the signal at site 1 was not fading below the 3 dB level. Furthermore, Fig. 12 shows that 87% of the fixed site fading below all levels occurred when the signal at site 1 was not attenuated by more than 2 dB. Such results demonstrate the obvious advantage of space diversity receiving techniques during periods of extremely dissimilar fading. However, for conditions of widespread rain activity of extent greater than the site separation, the measured attenuations at each site during the same time period may be similarly distributed as shown, for example, by the conditional distribution curves for period 7 given in Fig. 13. Here the duration of the attenuation below various levels at site 1 for specified levels at the fixed site is given. The curves tend to flatten out in the high attenuation range for all listed levels at the fixed site. This is a result of the time interval during which the received signal at site 1 was below the receiver threshold. Severe fading (below threshold) occurred for 22 sec at site 1 with the condition that the fixed site was already below the 6 dB level.

Of the seven rain periods analyzed, periods 4 and 7 showed the smallest measured diversity improvement. Nevertheless, two-site operation with 4 km site separation during these rain periods still

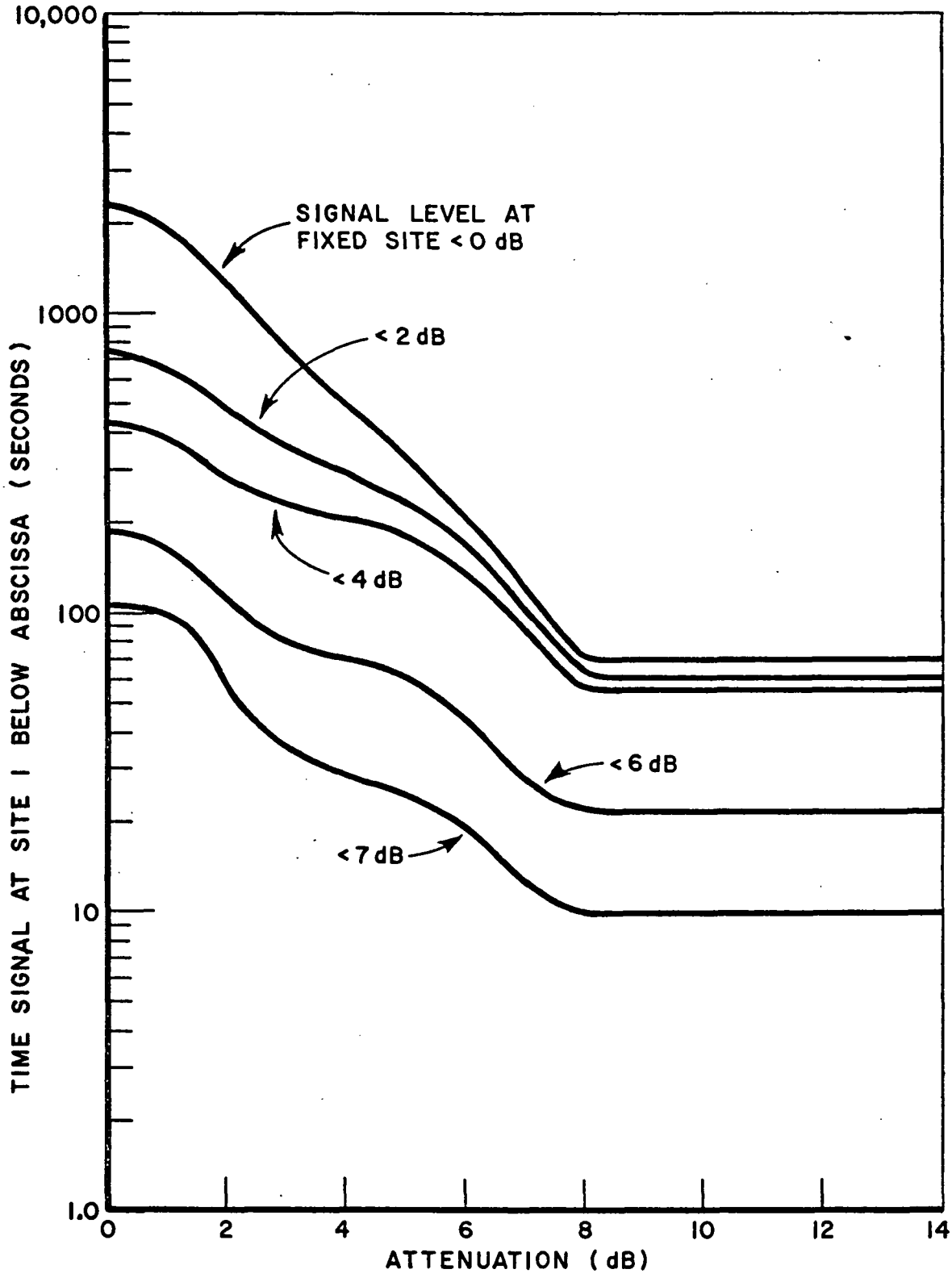

Fig. 13.--Conditional fade distribution for period 7.

provided a reduction in the duration of attenuation below the arbitrary 6 dB level by 78% in period 7 and by 70% in period 4 with respect to single-site durations below 6 dB.

D. Fade Durations

The fade events which characterize the received signal will have durations below given attenuation levels according to the duration and intensity of the rain rate along the path. The duration of a fade may be defined as the time during which the received signal remains continuously below a specified level. A cumulative distribution of fade durations experienced at the fixed site during the seven data periods is shown in Fig. 14. Here the values of the ordinate give the percentage of the number of fades which had durations exceeding the values of the abscissa. The total number of fades occurring at each level are also listed in the figure. The cross-over of the curves is a consequence of plotting percentages of the total number of fades at the specified level rather than the absolute numbers. The data shown in Fig. 14 is based on carrier data which has been averaged over 10 pulses.

Figure 15 gives the cumulative fade duration distributions for the data collected at site 1. The distributions of the fade durations tend to be similar at the two sites with, however, the fixed site suffering somewhat longer fade durations at the levels listed. The transportable terminal experienced a greater number of fades below 3 dB compared to the fixed site. The duration per fade at the 6 dB level was about the same for both sites. Fades below threshold tended to be longer at the fixed site; however, about half as many

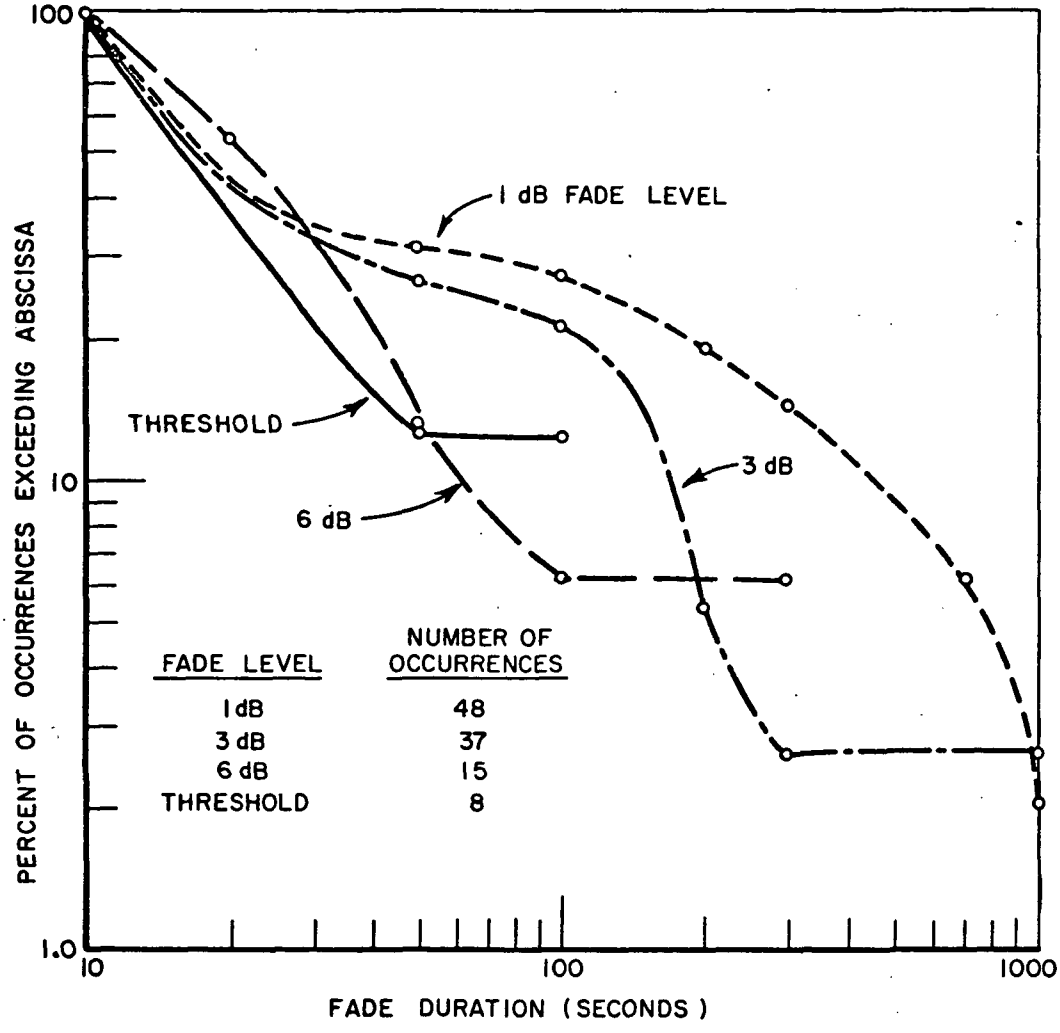

Fig. 14.--Cumulative fade distribution for fixed site.

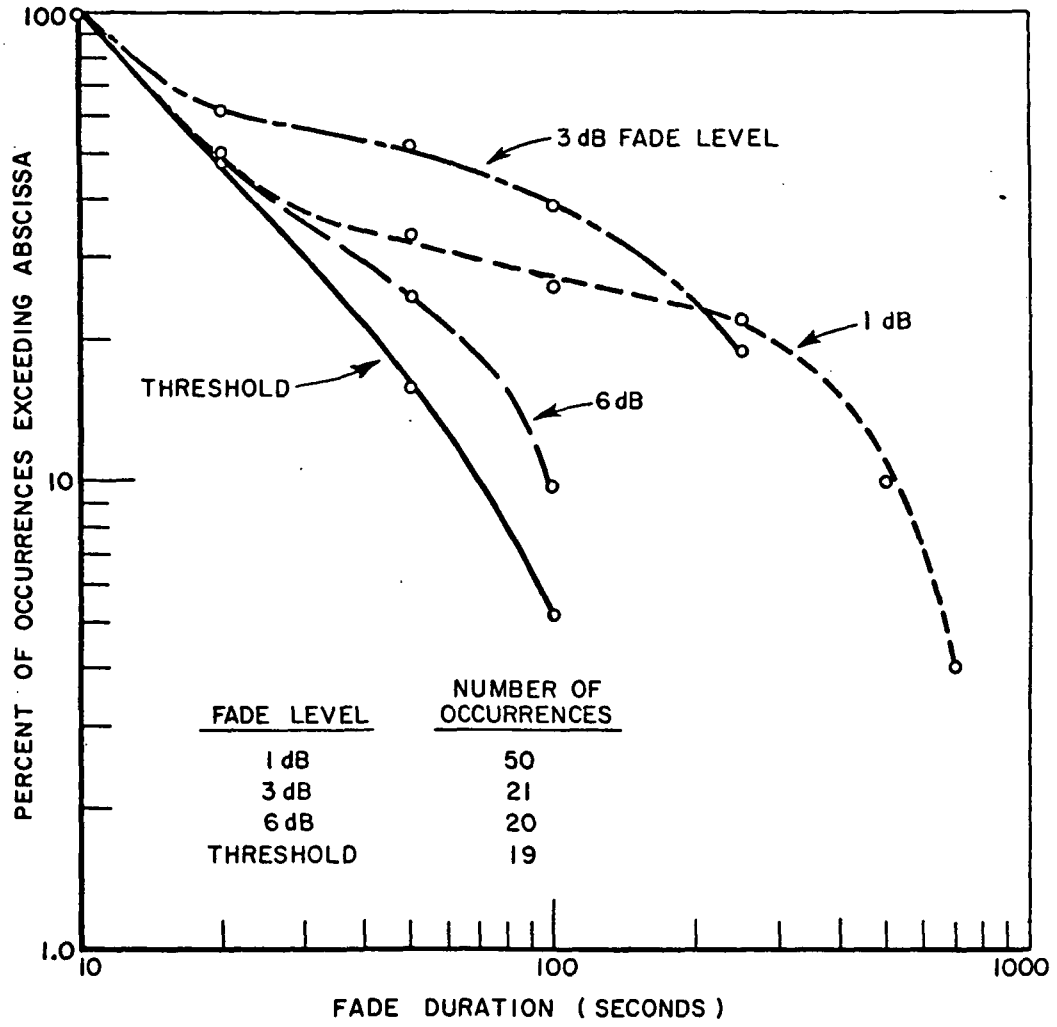

Fig. 15.--Cumulative fade duration distribution for site 1.

threshold level fades occurred at the fixed site. This result has probably been biased somewhat by the necessity of stowing the fixed site antenna during periods of high wind speeds.

The data shown in Figs. 14 and 15 have been replotted in Fig. 16 to show the relationship between the fade duration distri-

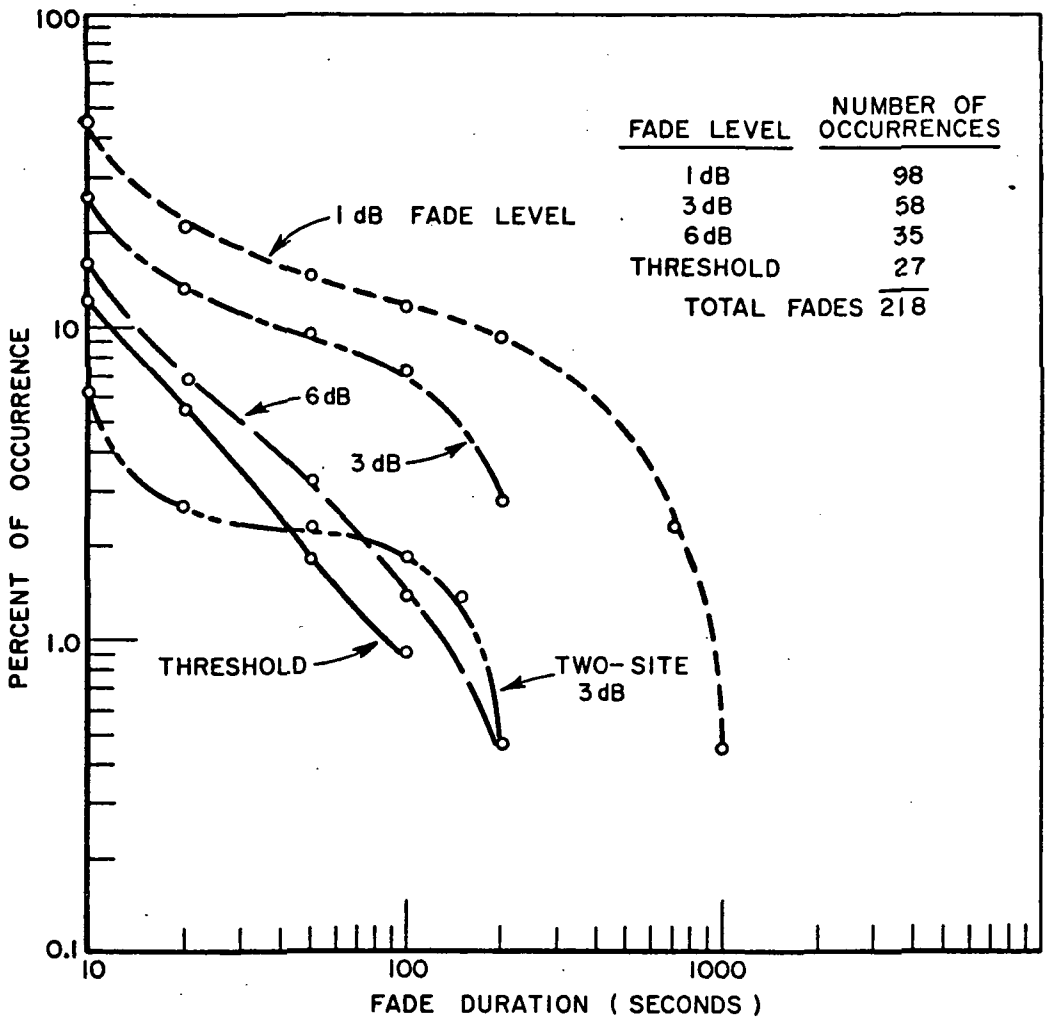

Fig. 16.--Cumulative fade duration distribution for single and two site fades.

butions observed at both sites. Twelve percent of all observed fades were at the threshold level or lower for durations of at least 10

seconds. Considering only the diversity fade periods analyzed, the longest single site fades at or below threshold were recorded during period 1 at site 1 and during period 2 at the fixed site and had durations of 125 and 154 seconds, respectively. Much longer single site threshold level fades have been observed during test runs when only one site was in operation. For example, on day 168 (see Fig. 5) the received signal level at site 1 was below threshold for 16.4 consecutive minutes beginning at approximately 0205Z. During this period the fixed site antenna was raised to protect it from high wind speeds.

Figure 16 also gives the duration distribution of 14 fades recorded when both sites remained simultaneously below the 3 dB fade level. These two-site fades below the 3 dB level occurred about one-half as frequently as total single site fades below the threshold level.

E. Correlation Between Attenuation and Radiometric Temperature

The correlation between the fading carrier signal and the path radiometric temperature must be established in order to use measured sky temperature data to predict attenuation reliably. The cross-correlation functions computed from measured radiometric temperature and received signal level data recorded during periods 1, 2, and 7 are shown in Figs. 17-19. High correlation ($\rho(0) \geq 0.8$) was obtained in each case and, of course, the delay time for maximum correlation was zero. Consequently, one may conclude that the path radiometric temperature measured using a narrow beam radiometer

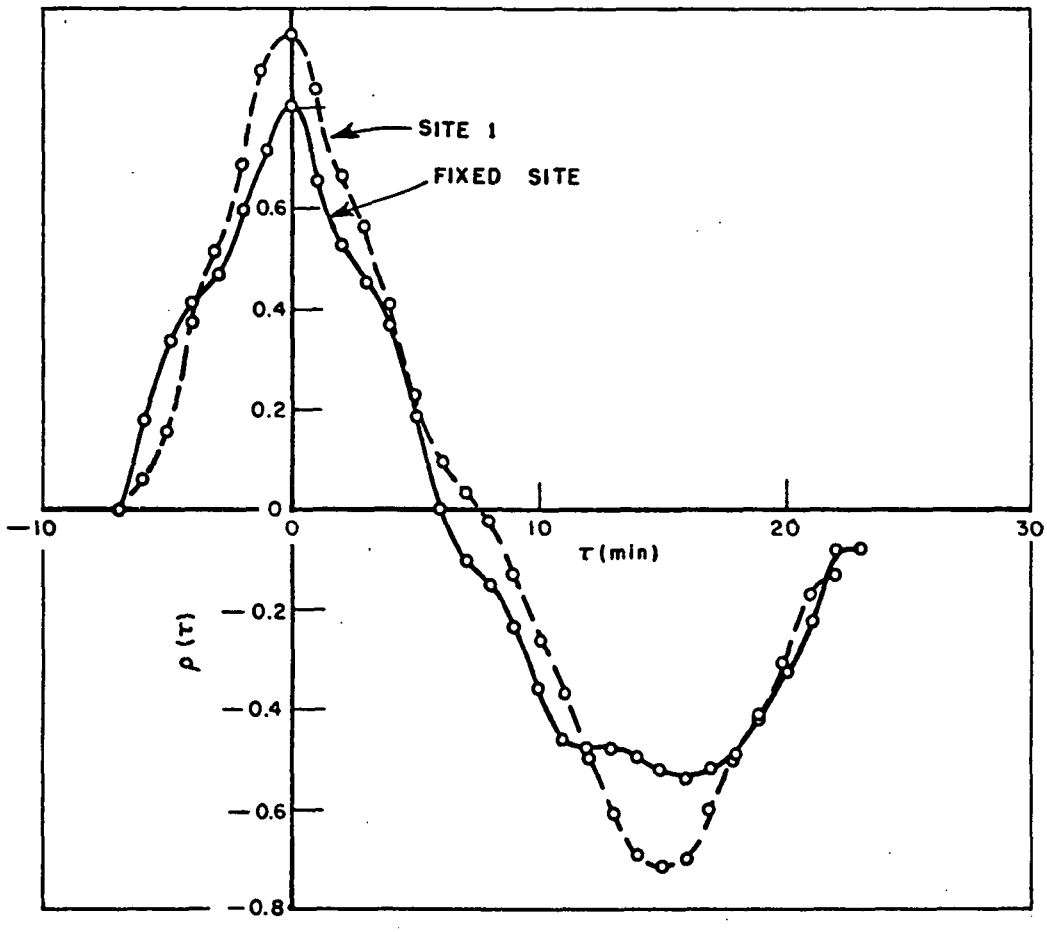

Fig. 17.--Cross-correlation between attenuation and radiometric temperature for period 1.

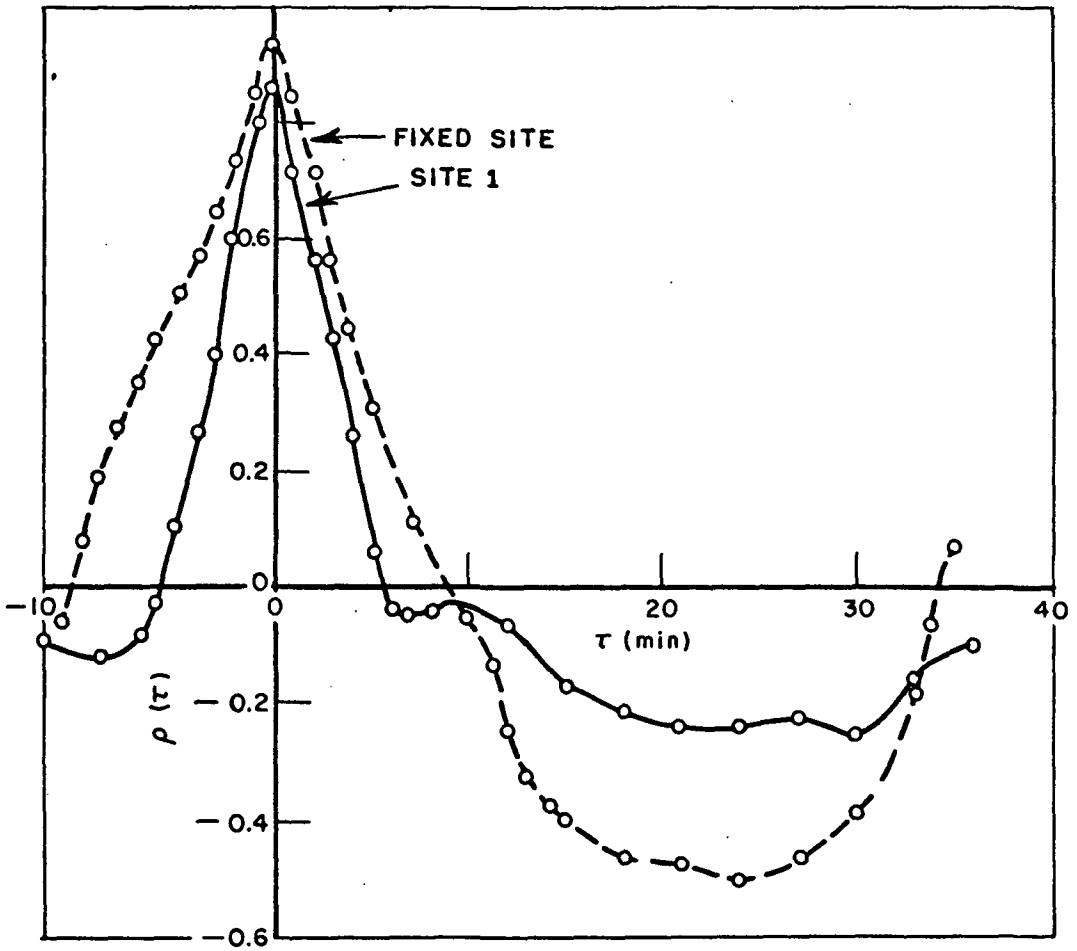

Fig. 18.--Cross-correlation between attenuation and radiometric temperature for period 2.

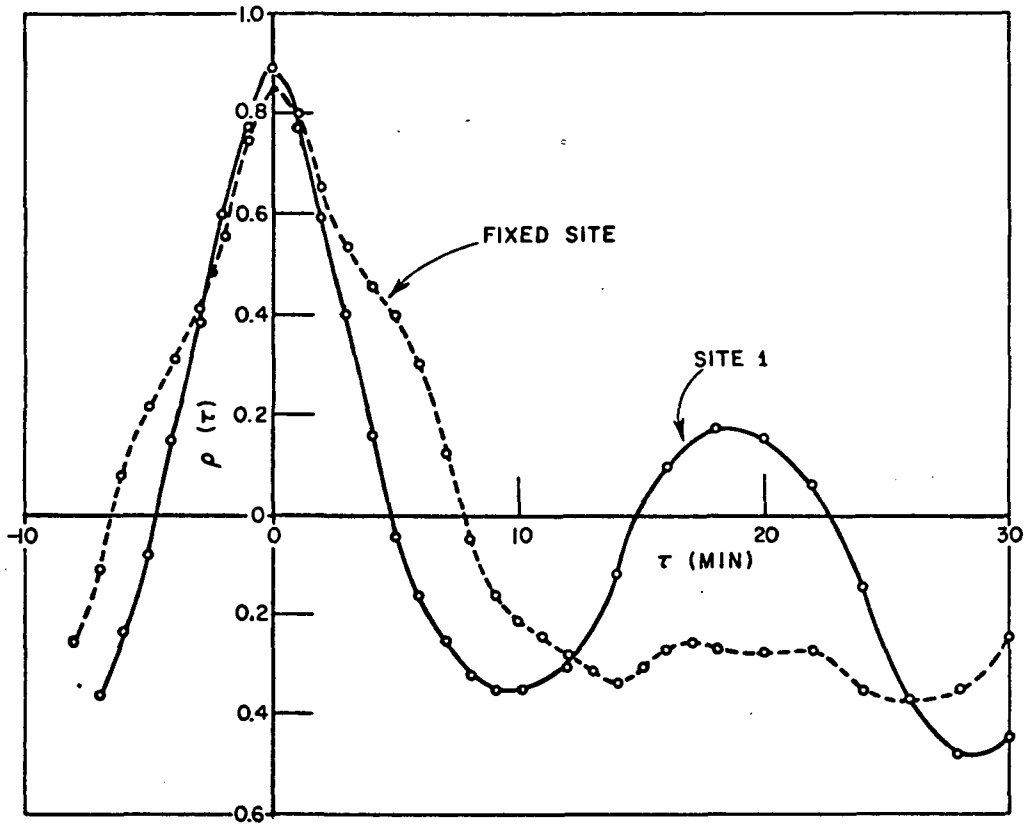

Fig. 19.--Cross-correlation between attenuation and radiometric temperature for period 7.

provides a reliable indicator of path attenuation over the dynamic range available in this experiment.

The value of the cross-correlation for zero delay does not reach unity due to: unavoidable antenna pointing errors, the non-linear relationship between attenuation and radiometric temperature, and the finite dynamic range of the PLL receiver. In this latter case the carrier was arbitrarily assigned the threshold level whenever its actual level was not known due to loss of receiver lock.

The results of the cross-correlation computations for the seven periods analyzed are shown in Table 3 along with the cumulative

TABLE 3

CROSS CORRELATION COEFFICIENTS BETWEEN ATTENUATION AND RADIOMETRIC TEMPERATURE DURING JUNE/JULY 1970 DATA PERIODS

PERIOD	DAY	$\rho_{xy}(0)$		REMARKS
		FIXED SITE	SITE 1	
1	166	.802	.961	
2	166	.942	.837	
3	168	.683	.866	Tracking Errors
4	168	.842	.902	
5	189	.202*	.753	Tracking Errors
6	189	.670	.743	Tracking Errors
7	196	.849	.896	
Cumulative	June/July 1970	.812	.923	

*Not used in cumulative totals due to significant tracking errors.

maximum cross-correlation value. The lower fixed site cumulative cross-correlation coefficient was due to tracking difficulties which resulted in additional apparent attenuation of the received signal level while having a negligible effect on the radiometric temperature measurement.

F. Correlation of Radiometric Temperature Between the Two Sites

Table 4 gives the results of the cross-correlation computations for the measured path temperatures at the two sites during the seven periods. The average correlation delay agrees closely with the average delay based on the measured attenuation data. The cumulative coefficient of cross-correlation computed from radiometric

TABLE 4

CROSS CORRELATION COEFFICIENTS OF MEASURED RADIOMETRIC TEMPERATURES ON EACH PATH DURING JUNE/JULY 1970 DATA

PERIOD	DAY	CROSS CORRELATION COEFFICIENT		LAG, τ(MIN)
		$\rho xy(\tau=0)$	MAX	
1	166	.632	.802	4 MIN
2	166	-.046	.867	8
3	168	.807	.807	0
4	168	.413	.451	2
5	189	.199	.423	3
6	189	.422	.455	0
7	196	.409	.598	3
Cumulative	June/July 1970	+.589	-	4.0 MIN

data is slightly higher than that computed from the attenuation data. This occurs since the radiometric temperature is not as strongly influenced by small antenna pointing errors and fades below threshold as is the coherent signal.

G. Mean Absorption Temperature

An empirical determination of the mean absorption temperature, T_m, based on measured attenuation and sky temperature data will assist in establishing the usefulness of Eq. (9) for predicting precipitation attenuation. Average values of T_m in each 1 dB attenuation interval over a total range of 10 dB using site 1 data from fade period 4 are given in Fig. 20. The number of satellite pulse samples used in averaging T_m in a particular interval is listed above the interval step, and the standard deviation of the T_m values from the computed mean is shown below the step. The high, physically unrealistic values of T_m for attenuations less than approximately

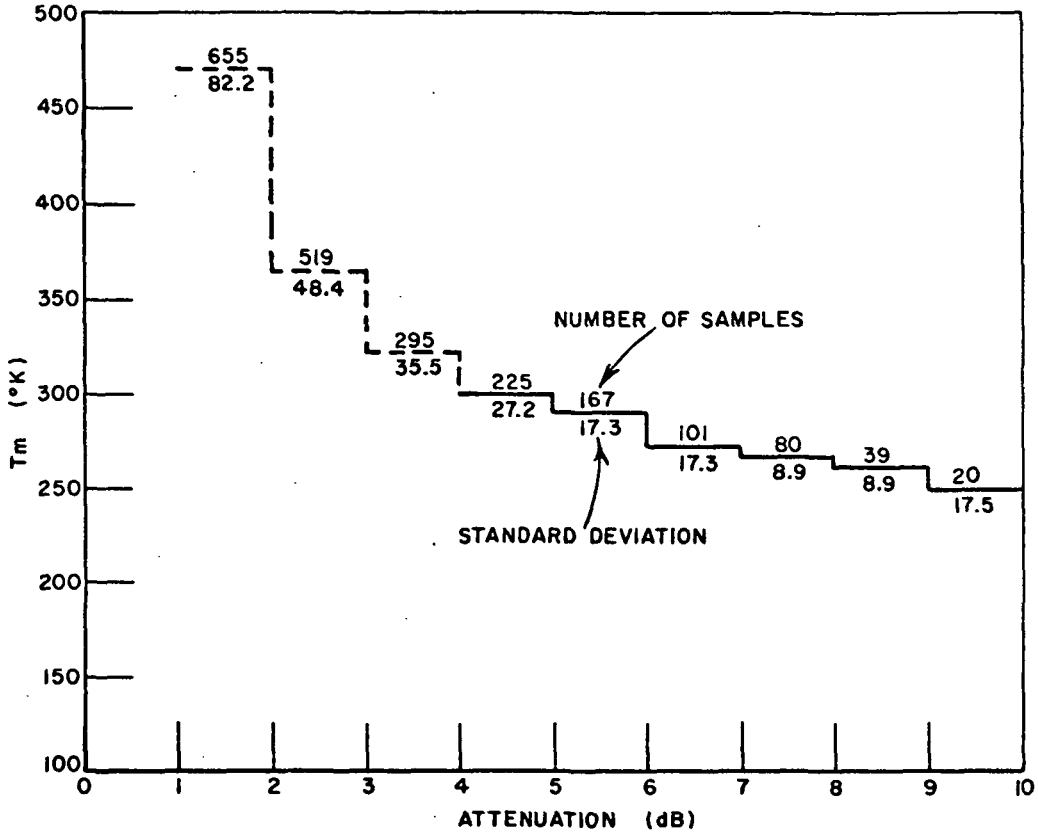

Fig. 20.--Empirical mean absorption temperature for various attenuation intervals from site 1 data for period 4.

4 dB are largely due to the uncertainties in the measured absolute level of the received signal as well as the rough assumption that T_B could be approximated by $T_{B_{eff}}$. In the high attenuation range T_m becomes critically dependent on the measurement accuracy of T_B. This can be seen from Eq. (9) as T_B approaches T_m.

Table 5 summarizes the cumulative average values of T_m in each 1 dB interval in the 4-10 dB range of attenuations for site 1 during the 1970 fade periods analyzed. A sufficient number of pulse samples is available in the cumulative total to substantiate

TABLE 5

MEAN ABSORPTION TEMPERATURES DETERMINED EMPIRICALLY USING ATTENUATION AND RADIOMETRIC TEMPERATURE AT SITE 1 DURING JUNE/JULY 1970 DATA PERIODS

ATTENUATION RANGE (dB)	T_m(°K)	No. SAMPLES
4-5 dB	302.1 °K	1076
5-6	285.9	731
6-7	284.5	498
7-8	277.7	297
8-9	271.9	145
9-10	265.2	76
4-10	T_m(AVE) = 281.2 °K	-

the trend for decreasing T_m with increasing attenuation as noted in Fig. 20. From the cumulative data in the table the empirically determined T_m appears to decrease by approximately 12% over the listed attenuation range.

A scatter plot of the received signal level versus the path radiometric temperature recorded at site 1 during the second fade event in period 3 (see Fig. 5) is presented in Fig. 21. Both the received signal and radiometric temperature are averaged over ten pulse intervals. Curves of the predicted attenuation as a function of path temperature using three values of T_m from Table 5 are shown as the solid traces. It can be seen that the empirically determined average value of T_m=281°K, based on attenuations in the 4-10 dB range, is effective for predicting measured attenuations with an error of approximately ±0.5 dB.

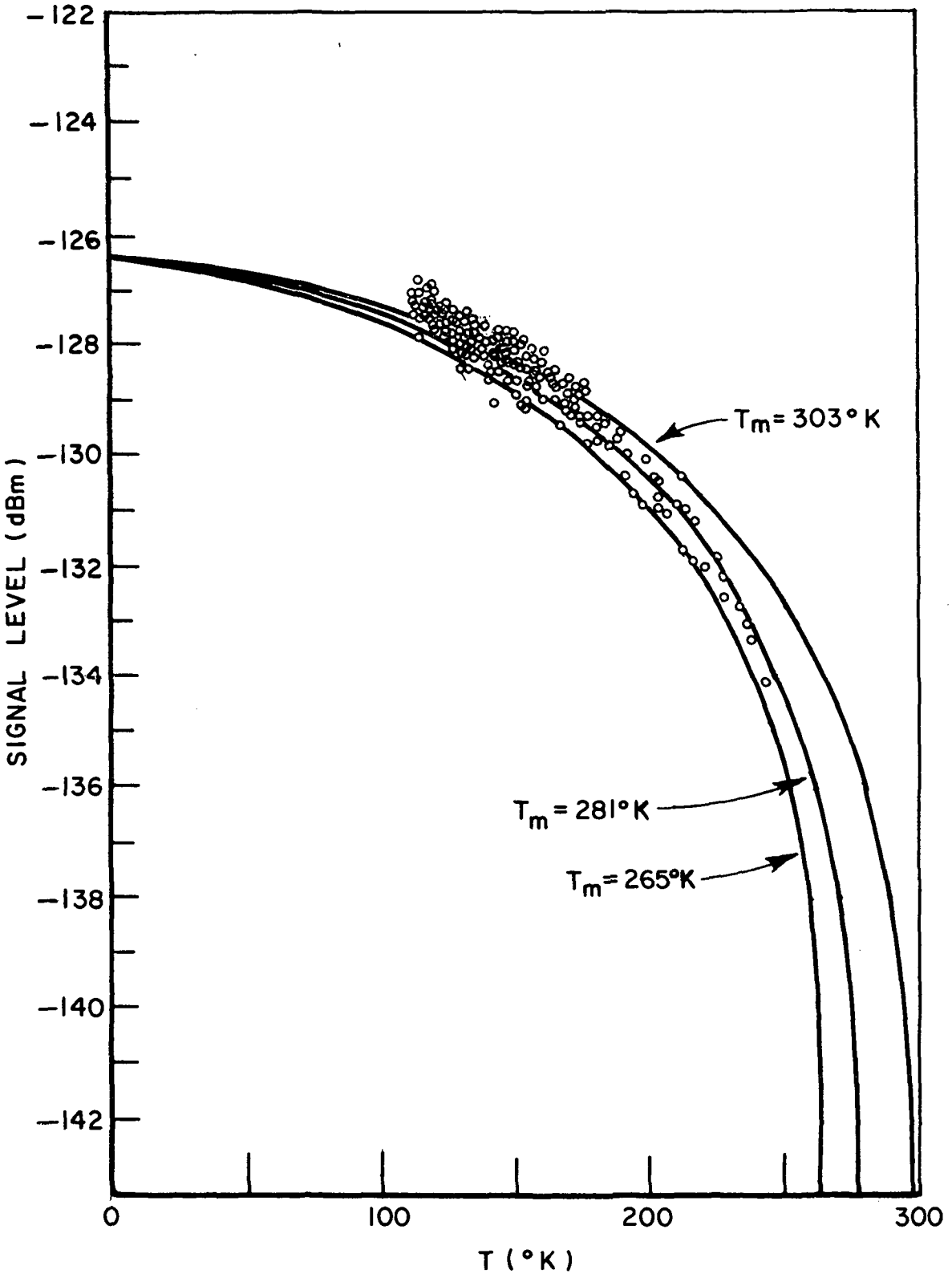

Fig. 21.--Received signal level vs radiometric temperature during 2315Z - 2330Z in period 3.

A comparison of mean absorption temperatures determined empirically and determined using the Wulfsberg expression, Eq. (12), is shown in Table 6. Site 1 data from 6 fade periods are considered.

TABLE 6

MEAN ABSORPTION TEMPERATURES PREDICTED AND EMPIRICALLY DERIVED FROM SITE 1 DATA

PERIOD	GMT	†CUMULATIVE T_m IN RANGE 4-10 dB (°K)	# SAMPLES	††PREDICTED T_m FOR GIVEN TIME (°K)
1	0611/0641Z	293.1 °K	603	276.2°K (0600Z) 276.2 (0700Z)
2	0941/1025	272.1	136	275.02 (0900Z) 275.6 (1000Z)
3	2224/2334	289.6	478	287.07 (2200Z) 284.5 (2300Z)
4	0128/0201	285.2	632	278.05 (0130Z) 280.0 (0200Z)
6	1924/2000	303.7	293	276.9 (1900Z) 276.3 (2000Z)
7	2224/2302	286.2	693	289.3 (2200Z) 284.8 (2300Z)

†Computed from Eq. (10) and based on measured attenuation and radiometric temperature.

††Computed from Wulfsberg Relation, Eq. (12).

The number of samples is the number of received pulses in the 4-10 dB range in each period. Values of T_m computed from the Wulfsberg equation are based on surface temperature data provided by the U.S. Weather Service at the times indicated. Except for periods 1 and 6, the empirical cumulative T_m in the 4-10 dB range agrees with

the Wulfsberg prediction to within the observed 12% variation in the empirically determined T_m (Fig. 21). Tracking errors during period 1 and insufficient higher attenuation data in period 6 contribute to the disagreement in these cases.

CHAPTER VI
SUMMARY

The results of space diversity propagation measurements made at the Ohio State University using the ATS-5 satellite and ground terminals separated by 4 km have been presented. The results of the fade distribution analysis have confirmed the effectiveness of the 4 km spacing in reducing the duration of fades greater than 6 dB by at least a factor of 10 during "worst-case" fading due to thunderstorm precipitation in June and July, 1970, at Columbus, Ohio. Furthermore, the results of the attenuation correlation analysis show that thunderstorm rain activity at the separated sites in these months produces fade events which have a cumulative coefficient of cross-correlation of 0.45 and are displaced in time by an average of 4.1 minutes.

Radiometric temperature data recorded at the transportable site using a narrow beam radiometer viewing the same atmospheric region as does the coherent channel antenna are highly correlated with the received signal level (greater than +0.85). These data together with the simple homogeneous Wulfsberg model may be used effectively to predict attenuation along elevated propagation paths. Empirical computations of the mean absorption temperature indicate that this approach is useful in predicting attenuations up to approximately 10 dB within an error of ±0.5 dB.

The space diversity technique has been shown to be a useful method for reducing the effects of precipitation attenuation at 15.3 GHz on satellite-to-ground paths and the effectiveness of the 4 km separation has been determined. The data acquisition and analysis effort at OSU are continuing during 1971 for a terminal separation of 8 km. In addition, the fixed site terminal has been upgraded by the installation of a more reliable 15 foot antenna which should substantially increase the data base for continuing diversity studies.

ACKNOWLEDGMENTS

The authors wish to acknowledge the assistance of several of their colleagues who spent extensive time fabricating, maintaining and operating the terminal equipment used in this research. The efforts of P. Bohley, R.C. Taylor, and M.D. Gordon are particularly appreciated. D.C. Upp and C.E. Prettyman wrote the original A/D computer program.

REFERENCES

1. Hogg, D.C., "Statistics on Attenuation of Microwaves by Intense Rain," Bell Systems Technical Journal, Vol. 48, November 1969.
2. Mondre, Erwin, "Atmospheric Effects on Millimeter Wave Communication Channels," NASA Document X-733-70-250, March 1970, p. 15.
3. Weibel, G.E. and Dressel, H.O., "Propagation Studies in Millimeter-Wave Link Systems," Proc IEEE, Vol. 55, April 1967, p. 497.
4. Van Vleck, J.H., "The Absorption of Microwaves by Oxygen," Phys. Rev., Vol. 71, No. 7, 1947, pp. 413-424.
5. Van Vleck, J.H., "The Absorption of Microwaves by Uncondensed Water Vapor," Phys. Rev., Vol. 71, No. 7, 1947, pp. 425-433.
6. Hogg, D.C., "Path Diversity in Propagation of Millimeter Waves Through Rain," IEEE Trans. Antennas Propagation, Vol. AP-15, May 1967.
7. Annual Status Report, "Millimeter-Wavelengths Propagation Studies," Report 2374-2, 1 November 1968, ElectroScience Laboratory, Department of Electrical Engineering, The Ohio State University; prepared under Grant No. NGR-008-080 for National Aeronautics and Space Administration.

8. Semiannual Status Report, "Millimeter-Wavelengths Propagation Studies," Report 2374-3, 15 April 1969, ElectroScience Laboratory, Department of Electrical Engineering, The Ohio State University; prepared under Grant No. NGR-008-080 for National Aeronautics and Space Administration.

9. Semiannual Status Report, "Millimeter-Wavelengths Propagation Studies," Report 2374-4, 30 April 1970, ElectroScience Laboratory, Department of Electrical Engineering, The Ohio State University; prepared under Grant No. NGR-008-080 for National Aeronautics and Space Administration.

10. Bohley, P. and Hodge, D.B., "Semiannual Status Report, "Millimeter-Wavelength Propagation Studies," Report 2374-5, 28 October 1970, ElectroScience Laboratory, Department of Electrical Engineering, The Ohio State University; prepared under Grant No. NGR-008-080 for the National Aeronautics and Space Administration.

11. Oguchi, T., private communication, cited by Oliver, T., "Atmospheric Attenuation and Sky Noise Temperature in the Microwave and Millimeter Wave Spectrum," Technical Report 2440-2, The ElectroScience Laboratory, Department of Electrical Engineering, The Ohio State University; prepared under Contract F33615-67-C-1663 for the Air Force Avionics Laboratory.

12. Medhurst, R.G., "Rainfall Attenuation of Cm Waves: Comparison of Theory and Measurement," IEEE Trans. Antennas Propagation, Vol. AP-13, July 1965.

13. Blevis, B.C., "Measurements of Rainfall Attenuation at 8 and 15 GHz," IEEE Trans. Antennas Propagation, Vol. AP-15, No. 3, May 1967.

14. Straiton, A.W., Scarpero, D.C., Vogel, W., "A Survey of Millimeter Wave Propagation Through the Atmosphere," Technical Report No. 68-1, Electrical Engineering Research Laboratory, University of Texas at Austin, 30 November 1968.

15. Gunn, K.L.S., and East, T.W.R., "The Microwave Properties of Precipitation Particles," Jour. Roy. Meteor Soc., Vol. 80, 1954.

16. Semplak, R.A., "The Influence of Heavy Rainfall on Attenuation at 18.5 and 30.9 GHz," IEEE Trans. Antennas Propagation, Vol. AP-18, No. 4, July 1970.

17. Wilson, R.W., "A Three-Radiometer Path-Diversity Experiment," Bell System Technical Journal, July-August 1970.

18. Altschuler, E.E., Wulfsberg, K.N., and Falcone, V.J., Jr., "Rain Attenuation at Millimeter Wavelengths," Air Force Cambridge Research Laboratories, Office of Aerospace Research, U.S. Air Force, L.G. Hanscom Field, Massachusetts.

19. Hogg, D.C. and Semplak, R.A., "Estimated Sky Temperatures Due to Rain for the Microwave Band," Proc. IEEE, March 1963, p. 499.

20. Wulfsberg, Karl N., "Apparent Sky Temperatures at Millimeter Wave Frequencies," Microwave Physics Laboratory, Project 4600, Air Force Cambridge Research Laboratories, Office of Aerospace Research, U.S. Air Force, L.G. Hanscom Field, Massachusetts.

21. Wilson, R.W., "Sun Tracker Measurements of Attenuation by Rain at 16 and 30 GHz," Bell System Technical Journal, Vol. 48, No. 5, May/June 1969, pp. 1383-1404.

22. Ippolito, L.J., "Millimeter Wave Propagation Measurements from the Applications Technology Satellite (ATS-V)," IEEE Trans. Antennas Propagation, Vol. AP-18, July 1970.

23. Binkley, Ippolito, King, and Ratliff, "The ATS-E Millimeter Wave Propagation Experiment," NASA/GSFC Report X-733-68-196, April 1968.

24. "Millimeter Wave Propagation Experiment, Participating Station Experiment Test Plan, Ohio State University, Columbus, Ohio," Westinghouse Electric Corp., Defense and Space Center, Baltimore, Maryland, January 1969.

25. Freeny, A.E. and Gabbe, J.D., "A Statistical Description of Intense Rain," Bell Systems Technical Journal, July-August 1969.

26. "ATS-V Millimeter Wave Propagation Experiment ATS Technical Data Report Quarterly Input, 6 April 1971, Contract No. NAS 5-21598, Westinghouse Electric Corporation.

27. Ippolito, L.J., "ATS-V Millimeter Wave Experiment Data Report," Vol. II, January-August 1970, NASA Document X-751-70-369, October 1970.

28. The Thunderstorm (Report of the Thunderstorm Project, U.S. Department of Commerce), Washington, D.C., 1949, p. 8.